Article

Bacterial chemolithoautotrophy via manganese oxidation

https://doi.org/10.1038/s41586-020-2468-5

Received: 26 September 2019

Accepted: 5 May 2020

Published online: 15 July 2020

Check for updates

Hang Yu[1] & Jared R. Leadbetter[1,2]✉

Manganese is one of the most abundant elements on Earth. The oxidation of manganese has long been theorized[1]—yet has not been demonstrated[2–4]—to fuel the growth of chemolithoautotrophic microorganisms. Here we refine an enrichment culture that exhibits exponential growth dependent on Mn(II) oxidation to a co-culture of two microbial species. Oxidation required viable bacteria at permissive temperatures, which resulted in the generation of small nodules of manganese oxide with which the cells associated. The majority member of the culture—which we designate '*Candidatus* Manganitrophus noduliformans'—is affiliated to the phylum Nitrospirae (also known as Nitrospirota), but is distantly related to known species of *Nitrospira* and *Leptospirillum*. We isolated the minority member, a betaproteobacterium that does not oxidize Mn(II) alone, and designate it *Ramlibacter lithotrophicus*. Stable-isotope probing revealed $^{13}CO_2$ fixation into cellular biomass that was dependent upon Mn(II) oxidation. Transcriptomic analysis revealed candidate pathways for coupling extracellular manganese oxidation to aerobic energy conservation and autotrophic CO_2 fixation. These findings expand the known diversity of inorganic metabolisms that support life, and complete a biogeochemical energy cycle for manganese[5,6] that may interface with other major global elemental cycles.

Beijerinck and Winogradsky discovered biological redox reactions involving carbon, nitrogen, sulfur and iron over a century ago, while pioneering methods for cultivating the microbiota responsible for these reactions: this led to the concept of chemolithoautotrophy[7,8]. The known breadth of inorganic electron-accepting and -donating reactions in biology has continued to expand[9–13]. For example, the anaerobic respiratory reduction of Mn(IV) oxides to Mn(II) by diverse microorganisms is now understood to be widespread and of broad biogeochemical importance[5,6,14,15]. Over the past century, a multitude of studies and reviews have focused on the details of Mn(II) oxidation catalysed by diverse heterotrophs[2–4]; however, the physiological roles of these activities generally remain unclear. Despite experimental hints that the oxidation might be coupled to energy conservation ($Mn^{2+} + 1/2O_2 + H_2O \rightarrow Mn(IV)O_{2(s)} + 2H^+$; $\Delta G^{o\prime} = -68$ kJ per mol Mn (Supplementary Note 1) in some organisms[1,16–19], whether Mn(II) oxidation drives the growth of any chemolithotrophs has remained an open question.

Cultivation of manganese oxidizers

We re-examined the possibility that previously unappreciated microorganisms from the environment might oxidize Mn(II) for energy. We coated a glass jar with a slurry of $Mn(II)CO_3$ and allowed it to dry, before filling it with municipal tap water from Pasadena (California, USA) and leaving it to incubate at room temperature. After several months, the cream-coloured carbonate coating had oxidized to a dark manganese oxide. We serially transferred the material into a defined medium, which led to the establishment of a stable in vitro culture. Unless otherwise noted, this medium was free of alternative organic and inorganic electron donors (except for trace amounts of vitamins); for example, nitrate was used instead of ammonia as a source of nitrogen to preclude the growth of nitrifiers.

To distinguish between abiological and biological oxidation, flasks of sterile, defined Mn(II) medium were either inoculated with a subculture of the enrichment or left uninoculated, and incubated under oxic conditions. Because manganese oxides have previously been suggested to contribute to the chemical auto-oxidation of Mn(II)[20], we inoculated other replicate flasks with a steam-sterilized subculture with oxide products. Even after a year, oxidation had not occurred in uninoculated flasks or flasks containing the steam-sterilized inocula, as predicted by the known chemical stability of $MnCO_3$ under these conditions[21,22]. However, within four weeks, the flasks inoculated with 'viable material' had generated dark, adherent manganese oxides (Fig. 1a). Oxidation required O_2 and occurred at temperatures up to 42 °C; oxidation occurring optimally between 34 °C to 40 °C (Extended Data Fig. 1a), consistent with catalysis being enzymatic. Mn(II) oxidation activity was also sensitive to exposure to antibiotics, or to overnight pasteurization at 50 °C (Extended Data Fig. 1b). Phosphate was inhibitory at concentrations above 0.3 mM. When amended with $MnCO_3$, the pH of unbuffered medium ranged between 5.7 and 6.3. Although a pH buffer was not required, Mn(II) oxidation was faster in medium buffered with 5 mM 3-morpholinopropanesulfonic acid (MOPS) at its pK_a (7.1 at 37 °C). In buffered cultures, the final pH ranged between 6.5 and 6.8. With or without buffer, increases in culture pH during or after oxidation—which

[1]Division of Geological and Planetary Sciences, California Institute of Technology, Pasadena, CA, USA. [2]Division of Engineering and Applied Science, California Institute of Technology, Pasadena, CA, USA. ✉e-mail: jleadbetter@caltech.edu

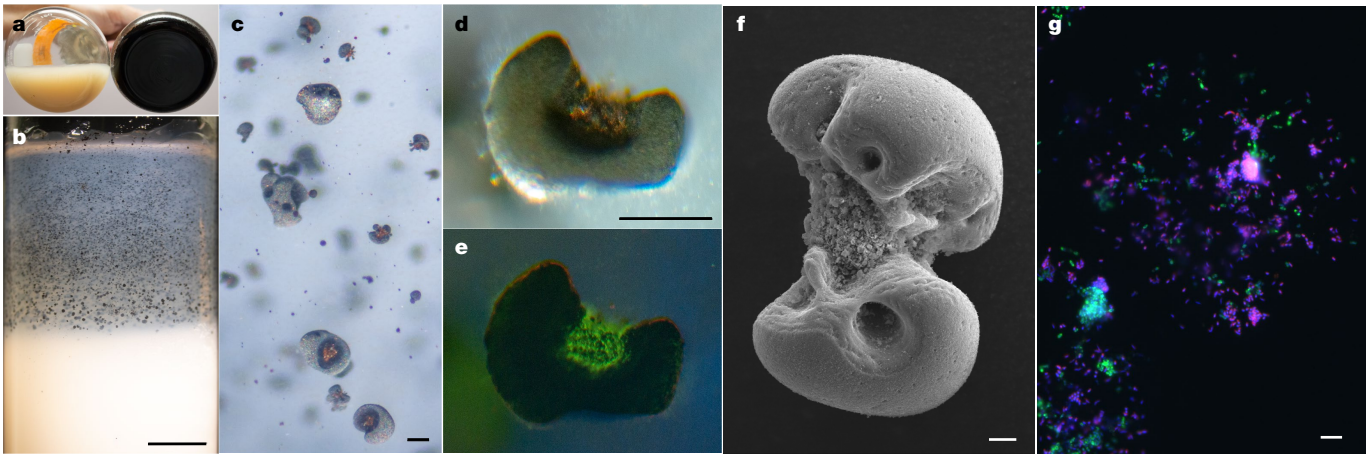

Fig. 1 | Bio-oxidation of $MnCO_3$ produces manganese oxide nodules to which two species associate. a, After incubation, comparison of an uninoculated control flask of basal medium containing bright, unreacted $MnCO_3$ (left) with the adherent dark oxide products generated in a flask that had been inoculated with viable material (right). **b**–**e**, Microscopy of manganese oxide nodules generated in agarose solidified $MnCO_3$ medium. **b**, After incubation of tubes inoculated with viable material, the cloud of bright $MnCO_3$ particles was clarified towards the air-exposed meniscus, concomitant with the generation of larger, discrete dark oxides (enlarged in **c**). **d**, Transmitted light micrograph of an acridine-orange (nucleic acid)-stained manganese oxide nodule from the same agarose tube. **e**, Epifluorescence micrograph of the same nodule as in **d**, with surface visible biomass localized to the inner clefts; material in clefts appeared orange before staining. **f**, Scanning electron micrograph of an manganese oxide nodule produced by the co-culture. **g**, Epifluorescence microscopy and fluorescence in situ hybridization using species-specific rRNA-targeted probes reveal cell distributions in dissolved manganese oxide nodules. Species A, magenta; species B, green; all DNA stained with DAPI, blue. No third species is present, via independent methods (Extended Data Fig. 3a). Each panel represents observations made from samples of multiple independent cultivation experiments (**a**, $n > 100$; **b**–**e**, $n = 7$; **f**, $n = 4$; and **g**, $n = 2$). Scale bars, 5 mm (**b**), 100 μm (**c**, **d**), 10 μm (**f**), 5 μm (**g**).

might lead to chemical oxidation of unreacted $MnCO_3$—were not observed. No growth could be detected in the MOPS-buffered basal medium without addition of $MnCO_3$ (Extended Data Fig. 2a).

An iTag community analysis of ribosomal RNA (rRNA) genes of the initial enrichment culture revealed about 70 different species, representing 11 bacterial phyla (Supplementary Table 1). The microorganisms responsible did not generate oxide-forming colonies on $MnCO_3$ agar plates, but successive rounds of serial dilution to extinction in $MnCO_3$ liquid medium refined the community to a co-culture of two species (which we designated species A and species B) (Supplementary Table 1). Species A belongs to the phylum Nitrospirae and species B is a betaproteobacterium; they occurred at a cell ratio of about 7:1 species A:species B (Extended Data Fig. 3a, Supplementary Table 1). Thus far, our attempts to isolate species A have failed. We isolated species B from disrupted oxides as single colonies on succinate and other heterotrophic media (Supplementary Note 2), but this species does not oxidize $MnCO_3$ alone. Either species A is solely responsible for Mn(II) oxidation (Extended Data Fig. 3b) or the activity is consortial (Extended Data Fig. 3c–e). Several members of the betaproteobacteria have previously proven recalcitrant to elimination from multispecies cultures: some were seemingly unimportant[9,23], whereas others engaged in metabolite cross-feeding[24], and in another they are central to a consortium[25].

DNA collected from both the co-culture and from a pure culture of species B produced near-complete genome sequences for both species (Extended Data Fig. 3f), which facilitated subsequent experiments and analyses.

Manganese oxide nodules

Mn(II) oxidation yielded morphologically conspicuous nodules of manganese oxide that were about 20–500 μm in diameter (Fig. 1, Extended Data Fig. 4). These nodules formed in both static and shaken liquid medium, often adhering to the glass and to each other, as well as in medium solidified with agarose (Fig. 1b). The surfaces were dark brown but often reflective, and typically invaginated around deeper depressions that had a rough, dark-orange surface (Fig. 1c, d). Attenuated total reflectance Fourier-transform infrared spectroscopy (ATR-FTIR) analysis revealed that the nodules of manganese oxide—after being bleached with hypochlorite to remove cellular and other organic carbon—are poorly ordered and similar to birnessite.

Our epifluorescence microscopic examination of nucleic-acid-stained nodules of manganese oxide found that the majority of the exposed biomass localized to the invaginations (Fig. 1d, e), with few cells being observed attached to the substrate or found to be planktonic. In agarose-solidified medium, these nodule-associated cells could be well-separated from the carbonate substrate, dissolving it from a distance (Fig. 1b). The latter is partially explained by the solubility products of the $MnCO_3$ precipitate; under the incubation conditions, these solubility products can be expected to include free Mn^{2+} ions, manganese bicarbonate and soluble $MnCO_3$[22]. The mean concentration of dissolved manganese in uninoculated and active $MnCO_3$ cultures was 0.214 mM (s.d. = 0.107, $n = 3$) and 0.119 mM (s.d. = 0.081, $n = 3$), respectively, before falling to 0.010 mM (s.d. = 0.009, $n = 3$) after oxidation. Soluble Mn(II) chloride does not appear to be used; instead, it appears to inhibit $MnCO_3$ oxidation when amended to active co-cultures at concentrations >2.0 mM (Extended Data Fig. 1c). No evidence for motility was observed: the oxides did not accumulate as a band across the interface between counter-opposing gradients of Mn(II) and O_2 in agarose-solidified medium (Fig. 1b), as is commonly observed for micro-aerophilic iron-oxidizing bacteria[26]. It is not yet understood whether the tight association of the cells with the oxidation product is circumstantial or is more intrinsic to the process, owing to some role of adsorptive, conductive, catalytic and/or other properties of manganese oxides.

Additional biomass was revealed upon chemical dissolution of the manganese oxide nodules; we examined this biomass using fluorescence in situ hybridization with specific rRNA-targeted probes (Supplementary Note 3). Consistent with the iTag analysis, cells of species A were more abundant than those of species B (Extended Data Fig. 3a). No stereotypic patterns of association with species B were observed (Fig. 1g, Extended Data Fig. 4a–e). Cells of both species

were often pleomorphic. Cells of species A were typically crescents, 1.07 μm by 0.40 μm (s.d. = 0.17 μm and 0.08 μm, respectively; $n = 50$); cells of species B were typically rods, 1.22 μm by 0.56 μm (s.d. = 0.20 μm and 0.09 μm, respectively; $n = 50$) in co-culture—but at high cell densities in pure cultures, the cells of species B elongate and form flocs.

Growth rates and yields

If one or both species in the co-culture is truly chemolithotrophic, the culture should exhibit (a) exponential increases in the rate of Mn(II) oxidation during and in parallel to (b) Mn(II)-dependent exponential growth. After inoculation, the rates of Mn(II) oxidation in the basal medium increased exponentially, initially doubling every 6.2 days (s.d. = 1.1, $n = 4$ replicate cultures) (Fig. 2a, Extended Data Fig. 2e–g, Supplementary Note 4) before decelerating to every 10.8 days (s.d. = 0.1). Concurrent with Mn(II) oxidation, species A exhibited sustained exponential growth, roughly matched by the less-numerous and perhaps-commensal species B (doubling every 6.1 and 7.7 days, respectively) (Fig. 2b, Extended Data Fig. 2b, Supplementary Note 5). The co-culture oxidized Mn(II) at a combined rate of 3.4 to 9.0×10^{-15} mol Mn(II) per cell per hour. We observed a linear relationship between Mn(II) oxidized by the co-culture and cell yields (Fig. 2c, Supplementary Note 6): 6.4×10^{11} cells of species A and 1.0×10^{11} cells of species B for a combined yield of 7.4×10^{11} cells per mol of Mn(II) oxidized. The total amount of DNA extracted from samples also increased exponentially with time and oxidation of Mn(II) (Extended Data Fig. 2c, d), yielding 3.1×10^6 ng DNA per mol of Mn(II) oxidized. On the basis of either of two estimates (both using the known dry weight of a single cell of *Escherichia coli*[27]), we estimate the growth yield in the co-culture to be between about 100 and 200 mg dry biomass per mol of Mn(II) oxidized. These growth yields and normalized substrate-oxidation rates are comparable with those observed for nitrite oxidation by chemolithotrophic microorganisms (Extended Data Fig. 3g), the metabolism of which is predicted to yield a free energy[12] similar to that calculated above for manganese oxidation.

Phylogenetic analyses

Species A affiliates remotely with the genera *Nitrospira*, *Leptospirillum* and other members of the phylum Nitrospirae, yet shares less than 84% 16S rRNA identity with any cultivated organism, and less than 87% identity to all but about 50 16S rRNA gene sequences from organisms that are as yet uncultivated (Fig. 3a, Extended Data Fig. 5a, c, Supplementary Table 2). The genome of species A does not encode recognizable genes for the chemolithotrophic oxidation of ammonia, hydroxylamine, nitrite or reduced sulfur compounds. Several closely related sequences have been recovered from drinking water and karst-affected groundwater, marine sites and a subsurface oxic–anoxic transition zone (Fig. 3a, Extended Data Fig. 5a). Together, these sequences cluster with '*Candidatus* Trogloglobea absoloni'[28], an uncultivated cave organism of unknown physiology. Few genome datasets are available for comparison. Species A shares less than 88% 16S rRNA gene identity to the best reference genomes (from metagenome-assembled genomes from groundwater[29,30]), and is the only genome currently available in the *Candidatus* class 'Trogloglia' (Fig. 3a, Extended Data Fig. 5b, c).

Species B affiliates with heterotrophs from the betaproteobacterial genus *Ramlibacter* (Extended Data Fig. 6a, b). It exhibited growth dependent on H_2 and O_2, encodes genes for hydrogenases, encodes both Sox and DsrMKJOP gene clusters for the oxidation of reduced sulfur, encodes a Calvin–Benson–Bassham cycle and may be capable of anaerobic respiration, such as denitrification and dissimilatory metal reduction. To our knowledge, the potential for facultative lithotrophy has not previously been reported for members of this genus.

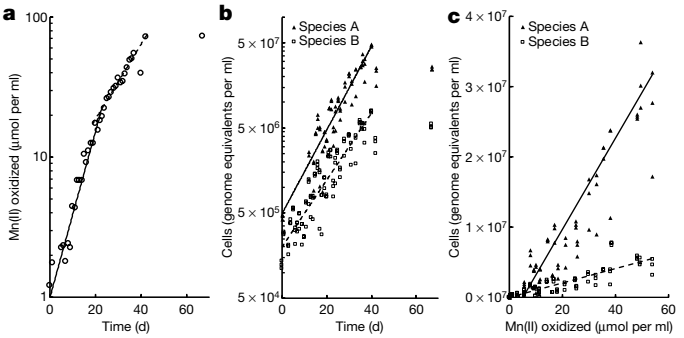

Fig. 2 | Mn(II) oxidation coupled to co-culture growth of species A and species B. a, Oxidation kinetics. Mn(II) oxidation rates increased exponentially over time in two distinct phases before plateauing. **b**, Growth kinetics. Exponential growth of species A and species B paralleled Mn(II) oxidation. **c**, Growth yield. Linear relationship between growth yield and the amount of Mn(II) oxidized. Points in **b**, **c** represent data from the three technical replicates for each sampled time point. Extended Data Fig. 2b–n provides analyses of independent cultivation experiments ($n = 9$).

Transcriptomics of manganese-dependent growth

We examined the transcriptomes of the co-culture (in particular, of species A), during different stages of Mn(II) oxidation in replicate cultures ($n = 7$) (Extended Data Fig. 3h). Although both species encode genes for swimming and twitching motility as well as for chemotaxis, these genes were not expressed (Supplementary Table 3)—matching the observations in agarose-solidified medium (see 'Manganese oxide nodules'). By contrast, biosynthetic genes for different compatibles solutes (for example, hydroxyectoine, trehalose and betaines) were expressed by both species and—consistent with this—co-cultures oxidized manganese when grown at a range of brackish salinities, up to nearly 40% of that of seawater.

We identified candidate genes that might underlie Mn(II) chemolithotrophy. Species A transcribed four gene clusters that encode outer membrane complexes that evoke comparisons with lithotrophic iron oxidizers and respiratory metal reducers. By analogy, these gene clusters might have a role in extracellular electron transfer by ferrying Mn(II)-derived electrons to periplasmic carriers (candidates for which were also expressed; Supplementary Table 4), leaving the resultant insoluble oxide outside the cell (Fig. 3b). In iron-oxidizing microorganisms, an outer membrane *c*-type cytochrome (Cyc2 or Cyt572) is often used as the initial oxidant and carrier for the Fe(II)-derived electron[31,32]. Species A expressed a Cyc2 homologue with a predicted haem-binding site and outer-membrane β-barrel structure (Fig. 3b, Supplementary Table 4). In iron-oxidizing anoxygenic phototrophs[33,34] and in several neutrophilic iron-oxidizing chemolithotrophs[35], an alternative mechanism involves a porin–cytochrome *c* protein complex[36]. Species A expresses genes for three recognizable porin–cytochrome *c* protein complexes: a porin–dodecaheme cytochrome *c* with no homologues in the databases (labelled PCC 1) and two distinct porin–decaheme cytochrome *c* modules (labelled PCC 2 and PCC 3) (Fig. 3b). During growth in the Mn(II)-oxidizing co-culture, species B expresses an MtrA–MtrB–MtrC-like porin–cytochrome *c* protein complex, as well as other multihaem cytochrome *c* proteins with a greater resemblance to the complexes involved in anaerobic reduction of metals by *Shewanella* sp.[36] (Supplementary Table 5).

After the transfer of Mn(II)-derived electrons from outside of the cell into the periplasm, their flow through respiratory complexes in the cytoplasmic membrane is central to understanding this mode of energy conservation. On average, the two Mn(II)-derived electrons are generally considered to be of high potential (Mn(II)/Mn(IV), $E^{0\prime} = +466$ mV, Supplementary Note 1). However, the energetics of each of the two

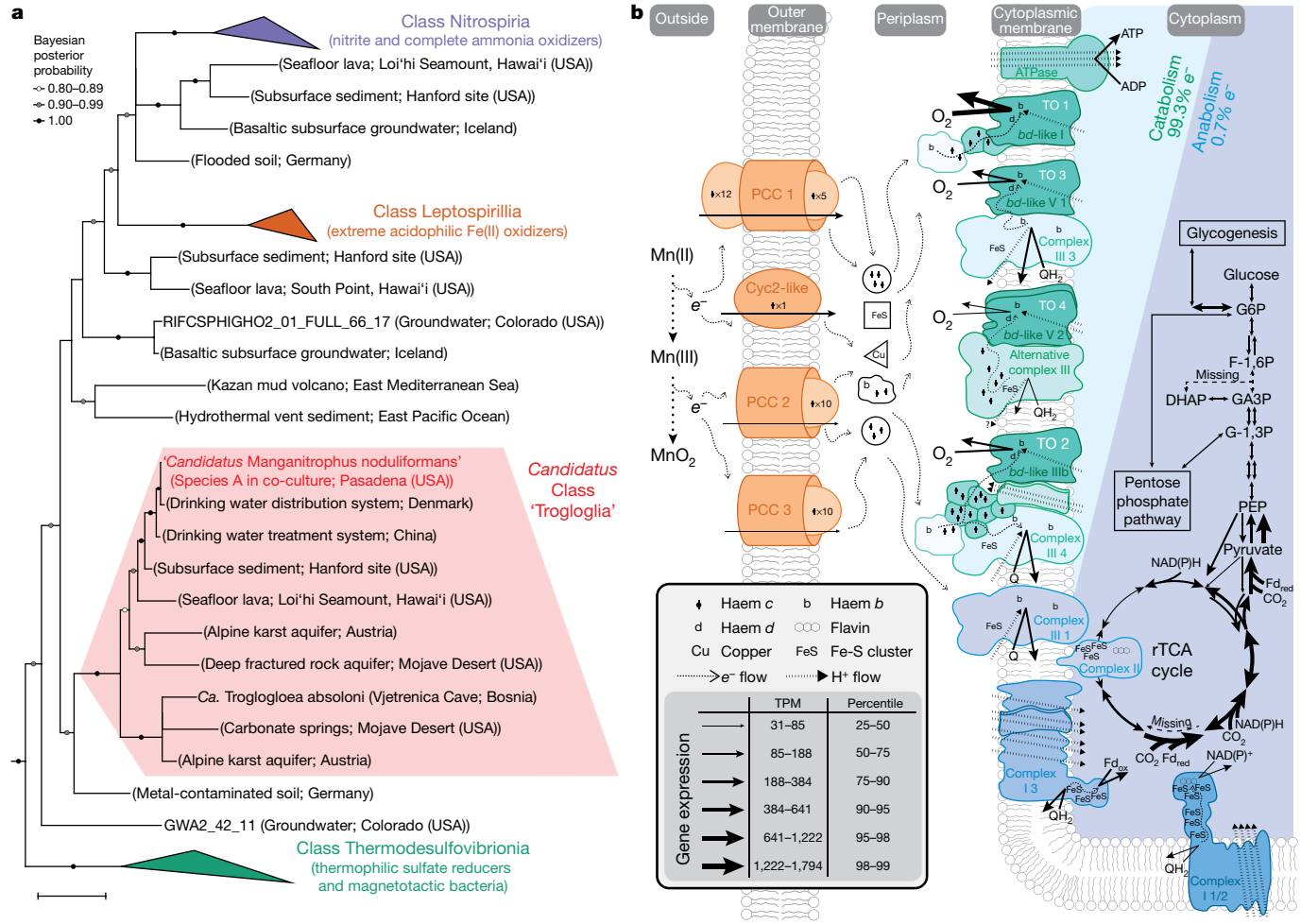

Fig. 3 | Phylogenetic analysis and metabolic reconstruction of species A ('*Candidatus* Manganitrophus noduliformans'). **a**, Bayesian phylogram based on 1,532 aligned 16S rRNA nucleotide positions. Sequences clustering within the three previously described classes within the bacterial phylum Nitrospirae are collapsed into separate nodes. Species A clusters with not-yet-cultivated members of the Trogloglia, a distinct class within this phylum. Extended Data Fig. 5a–c provides greater detail and identifiers. Scale bar shows evolutionary distance (0.1 substitutions-per-site average). **b**, Hypothetical model of e^- flow from extracellular Mn(II) to the energy and anabolic systems of species A. The oxidation is hypothesized to be mediated by several expressed outer membrane complexes (orange), with subsequent e^- transfers to periplasmic carriers. The bulk of e^- flow is towards generating proton motive force via terminal oxidases (TO) (green) during O_2 respiration. The remaining e^- flow would be to motive force-dissipating, reverse electron transport complexes (blue), generating the low-potential e^- carriers required for CO_2 fixation mediated by the rTCA pathway. Gene-expression values represent the mean of independent cultivation experiments ($n = 7$). Supplementary Table 4 provides identifiers and transcript levels for each gene, and Supplementary Notes 7 and 8 provide more detailed explanations of the diagrams. TPM, transcripts per million.

sequential one-electron transfers can be affected by inorganic and organic binding ligands[22,37], leading to a degree of uncertainty. Of the respiratory complexes, canonical respiratory complex I is unlikely to be used for energy conservation; this leaves canonical or alternative complex III, complex IV or cytochrome *bd* oxidases as possible candidates for generating a proton motive force during Mn(II) chemolithotrophy.

The genome of species A contains host gene clusters for terminal oxidases that could link the quinone pool to O_2; many of these gene clusters are strongly transcribed (Supplementary Table 4). Although a role in the process cannot be ruled out, the single complex IV (a Cbb3-type cytochrome *c* oxidase) of species A is not as well-expressed (in the 24th percentile) as four unconventional terminal-oxidase complexes that contain cytochrome *bd*-like oxidase (Fig. 3b, Extended Data Figs. 7, 8, Supplementary Table 4, Supplementary Note 7). The most highly expressed of these terminal oxidases is 'TO 1' (in the 99th percentile) (Fig. 3b), a complex that is generally similar to those observed in ammonia- and nitrite-oxidizing members of the Nitrospirae[38,39] but without the hypothesized candidate catalytic and iron–sulfur subunits NxrA and NxrB. The second highest expressed terminal oxidase ('TO 2') (in the 83rd percentile) also lacks these subunits, and is highly unusual amongst cultivated organisms in containing extra haem *c* domains, cytochrome *c* and two MrpD-like ion-pumping subunits (Fig. 3b, Supplementary Table 4) that might—hypothetically—facilitate electron transfer while generating a motive force. In both TO 1 and TO 2, a membrane-attached di-haem cytochrome *b* may connect extracellular electron transfer and periplasmic electron carriers to these membrane complexes (Fig. 3b, Supplementary Note 7). Whether either of these will have a high affinity for O_2 (as canonical cytochrome *bd*-oxidases do) is not known. Future studies are required to examine the function of these unusual terminal oxidases, their roles in energy conservation and how any energetic challenge of the initial oxidation of Mn(II) to Mn(III) is offset or met by the organism.

Mn(II)-oxidation-dependent CO_2 fixation

With the demonstration that Mn(II) oxidation drives lithotrophic energy metabolism and growth, we examined whether the co-culture might generate biomass via autotrophic CO_2 fixation with Mn(II)-derived

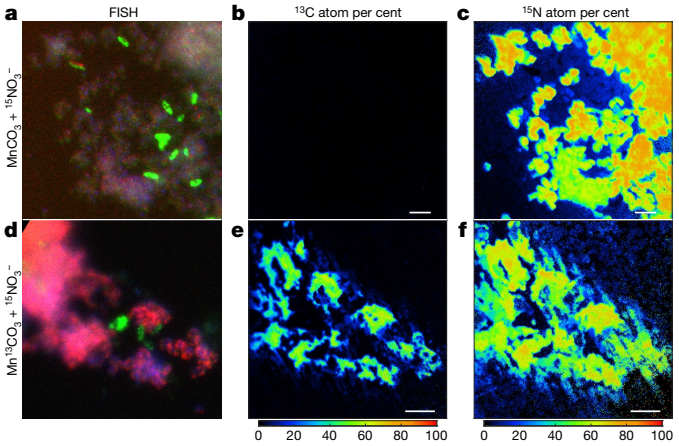

Fig. 4 | Stable isotope probing of autotrophic CO_2 fixation. We compared cells grown in the basal medium with labelled $Mn^{13}CO_3$ and $^{15}NO_3^-$ to cells grown with unlabelled $MnCO_3$ and $^{15}NO_3^-$. **a**, **d**, Fluorescence in situ hybridization (FISH) of cells dissolved from manganese oxide nodules using species-specific rRNA-targeted probes. Species A, magenta; species B, green; all DNA stained with DAPI, blue. **b**, **c**, **e**, **f**, Nanometre-scale secondary-ion mass spectrometry (nanoSIMS) reveals incorporation of ^{13}C and ^{15}N into cells. Coloured scale bars indicate ^{13}C or ^{15}N atom per cent. Scale bars, 3 µm. Areas shown in **b**, **c** and **e**, **f** correspond to those in **a** and **d**, respectively. Extended Data Fig. 9a shows analyses of independent nanoSIMS images ($n = 5$) from the same culture incubated with inorganic ^{13}C.

electrons. For this, we grew the co-culture with labelled ^{13}C-$MnCO_3$ (and ^{15}N-nitrate to aid in tracking the synthesis of new biomass) and visualized the isotopic compositions of cells microscopically by species-specific fluorescence in situ hybridization coupled to nanometre-scale secondary-ion mass spectrometry (nanoSIMS) (Fig. 4). The results are consistent with the co-culture being autotrophic. Both species A and species B were confirmed to incorporate substantial amounts of ^{13}C and ^{15}N isotopes (Fig. 4, Supplementary Note 9). Species A showed a higher enrichment for both isotopes as compared to species B (Extended Data Fig. 9a), which suggests that it is the main—if not sole—driver of Mn(II)-dependent CO_2 fixation and lithoautotrophic growth in the co-culture (especially when taken together with its greater abundance, as shown in Extended Data Fig. 3a). Although we cannot rule out the possibility that a degree of anabolic mixotrophy might occur via the uptake of trace contaminating organic carbon, it is likely that species A has an inoperable oxidative TCA cycle: it does not encode a recognizable homodimeric 2-oxoglutarate dehydrogenase complex (Fig. 3b, Supplementary Note 10), which is a hallmark deficiency that has been observed in many autotrophs that are unable to mineralize organic carbon (including nitrogen- and iron-oxidizing members of the Nitrospirae, which grow autotrophically using the reverse tricarboxylic acid (rTCA) pathway[38,40,41]).

During Mn(II)-dependent growth in the co-culture, species A expresses genes for a complete rTCA pathway (Fig. 3b, Supplementary Table 4, Supplementary Note 10). Although the role of the Calvin–Benson–Bassham cycle in manganese oxidation is speculative, species B expresses genes for this cycle (Supplementary Table 5).

For species A to fix CO_2 via the rTCA pathway, low-potential electron carriers (for example, $NAD(P)^+$ and ferredoxin)[42] need to be reduced with high-potential Mn(II)-derived electrons, possibly via a reverse electron transport chain that—at the very least—involves complex I (Fig. 3b). Three distinct complex I gene clusters can be found in species A, two of which (complex I 1 and complex I 2) (Fig. 3b, Supplementary Table 4) hypothetically might dissipate energy when operated in reverse and generate NAD(P)H ($E^{\circ\prime} = -320$ mV)[43] from reduced quinones with a more-positive reduction potential. Similarly, an unusual complex I (complex I 3) (Fig. 3b, Supplementary Table 4) might be used to reduce ferredoxin ($E^{\circ\prime} = -398$ mV)[43]. This complex encodes five ion-pumping subunits (NuoN, two NuoM and two MrpD-like subunits, but no NuoL), whereas the canonical complex I only encodes three (NuoL, NuoM and NuoN)[44]. Rare and unusual variants of complex I with four ion-pumping subunits (NuoL, two NuoM and NuoN) have recently been identified and postulated to couple the inward flow of five protons to drive the endergonic reduction of ferredoxin from a quinone[45,46]. In species A, complex I 3 hypothetically may use electrons from the quinone pool to drive the reduction of ferredoxin via the inward flow of six protons or ions (Fig. 3b). If the entry point(s) of Mn(II)-derived electrons into the electron transport chain has a reduction potential more positive than that of the quinone pool, then additional respiratory complexes (Fig. 3b) would have to be involved to accomplish productive reverse electron flow (Supplementary Note 7).

Discussion

Whether chemolithoautotrophic manganese-oxidizing microorganisms exist had been an open question for over a century[1–4]. This study establishes their existence, and provides insights into the details and dynamics of the process at cellular, physiological, genomic, transcriptomic and isotopic levels. Manganese chemolithoautotrophy extends the known physiologies in the phylum Nitrospirae that leverage meagre differences in redox potential between inorganic electron donors and acceptors[9,12,47–49]. On the basis of physiology, phylogeny, genomics and other characteristics of species A, we propose the epithet '*Candidatus* Manganitrophus noduliformans' for this species (taxonomic proposal in Supplementary Information).

The potential effect of Mn(II) oxidation coupled with the seemingly slow exponential growth of the co-culture (Extended Data Fig. 3g) has current and past environmental implications. Starting with a single cell each of species A and B, unrestricted chemolithotrophic growth at the observed cell doubling times and oxidation rates would be sufficient to generate manganese oxides that equal global manganese reserves within two years (Supplementary Note 11). On the basis of phylogenetic inferences, close relatives of species A reside in many subsurface and karst environments (Fig. 3a, Extended Data Fig. 5a), including at oxic–anoxic transition zones such as the Hanford sediments[50]. At such interfaces, manganese could be cycled between aerobic Mn(II)-oxidizing chemolithoautotrophs and anaerobic, manganese-oxide-respiring (reducing) chemotrophs[5,6,14,15], thereby stimulating substantial electron flows through the element over even-brief geological time scales. This has implications for the interconnected biogeochemical cycles of carbon, nitrogen, sulfur, iron, hydrogen and oxygen, with which this complete manganese energy cycle could interact.

Online content

Any methods, additional references, Nature Research reporting summaries, source data, extended data, supplementary information, acknowledgements, peer review information; details of author contributions and competing interests; and statements of data and code availability are available at https://doi.org/10.1038/s41586-020-2468-5

1. Beijerinck, M. Oxydation des mangancarbonates durch Bakterien und Schimmelpilze. *Folia Microbiol. (Delft)* **2**, 123–134 (1913).
2. Nealson, K. H., Tebo, B. M. & Rosson, R. A. Occurrence and mechanisms of microbial oxidation of manganese. *Adv. Appl. Microbiol.* **33**, 279–318 (1988).
3. Tebo, B. M., Johnson, H. A., McCarthy, J. K. & Templeton, A. S. Geomicrobiology of manganese(II) oxidation. *Trends Microbiol.* **13**, 421–428 (2005).
4. Hansel, C. & Learman, D. R. in *Ehrlich's Geomicrobiology* (eds Ehrlich, H. L. et al.) 401–452 (CRC, 2015).
5. Myers, C. R. & Nealson, K. H. Bacterial manganese reduction and growth with manganese oxide as the sole electron acceptor. *Science* **240**, 1319–1321 (1988).
6. Lovley, D. R. & Phillips, E. J. Novel mode of microbial energy metabolism: organic carbon oxidation coupled to dissimilatory reduction of iron or manganese. *Appl. Environ. Microbiol.* **54**, 1472–1480 (1988).
7. Winogradsky, S. Über schwefelbakterien. *Bot. Ztg* **45**, 489ff (1887).

8. Kelly, D. P. & Wood, A. P. in *The Prokaryotes: Prokaryotic Communities and Ecophysiology* (eds Rosenberg, E. et al.) 275–287 (Springer, 2013).
9. Daims, H. et al. Complete nitrification by *Nitrospira* bacteria. *Nature* **528**, 504–509 (2015).
10. Könneke, M. et al. Isolation of an autotrophic ammonia-oxidizing marine archaeon. *Nature* **437**, 543–546 (2005).
11. Strous, M. et al. Missing lithotroph identified as new planctomycete. *Nature* **400**, 446–449 (1999).
12. van Kessel, M. A. H. J. et al. Complete nitrification by a single microorganism. *Nature* **528**, 555–559 (2015).
13. Watson, S. W. & Waterbury, J. B. Characteristics of two marine nitrite oxidizing bacteria, *Nitrospina gracilis* nov. gen. nov. sp. and *Nitrococcus mobilis* nov. gen. nov. sp. *Arch. Mikrobiol.* **77**, 203–230 (1971).
14. Lovley, D. R., Holmes, D. E. & Nevin, K. P. in *Advances in Microbial Physiology* (ed Poole, R. K.) 219–286 (Elsevier, 2004).
15. Henkel, J. V. et al. A bacterial isolate from the Black Sea oxidizes sulfide with manganese(IV) oxide. *Proc. Natl Acad. Sci. USA* **116**, 12153–12155 (2019).
16. Ghiorse, W. C. & Ehrlich, H. L. Microbial biomineralization of iron and manganese. *Catena Suppl.* **21**, 75–99 (1992).
17. Ehrlich, H. L. & Salerno, J. C. Energy coupling in Mn^{2+} oxidation by a marine bacterium. *Arch. Microbiol.* **154**, 12–17 (1990).
18. Ehrlich, H. L. Manganese as an energy source for bacteria. Environ. *Biogeochem.* **2**, 633–644 (1976).
19. Dick, G. J. et al. Genomic insights into Mn(II) oxidation by the marine alphaproteobacterium *Aurantimonas* sp. strain SI85-9A1. *Appl. Environ. Microbiol.* **74**, 2646–2658 (2008).
20. Nealson, K. H. in *The Prokaryotes* (eds Dworkin, M. et al.) 222–231 (Springer, 2006).
21. van Veen, W. L. Biological oxidation of manganese in soils. *Antonie van Leeuwenhoek* **39**, 657–662 (1973).
22. Morgan, J. J. Kinetics of reaction between O_2 and Mn(II) species in aqueous solutions. *Geochim. Cosmochim. Acta* **69**, 35–48 (2005).
23. Kits, K. D. et al. Kinetic analysis of a complete nitrifier reveals an oligotrophic lifestyle. *Nature* **549**, 269–272 (2017).
24. Flagan, S. F. & Leadbetter, J. R. Utilization of capsaicin and vanillylamine as growth substrates by *Capsicum* (hot pepper)-associated bacteria. *Environ. Microbiol.* **8**, 560–565 (2006).
25. Kanzler, B. E. M., Pfannes, K. R., Vogl, K. & Overmann, J. Molecular characterization of the nonphotosynthetic partner bacterium in the consortium *"Chlorochromatium aggregatum"*. *Appl. Environ. Microbiol.* **71**, 7434–7441 (2005).
26. Emerson, D. & Moyer, C. Isolation and characterization of novel iron-oxidizing bacteria that grow at circumneutral pH. *Appl. Environ. Microbiol.* **63**, 4784–4792 (1997).
27. Neidhardt, F. C. Escherichia coli *and* Salmonella*: Cellular and Molecular Biology*, vol. 1 (ASM, 1996).
28. Kostanjšek, R., Pašić, L., Daims, H. & Sket, B. Structure and community composition of sprout-like bacterial aggregates in a dinaric karst subterranean stream. *Microb. Ecol.* **66**, 5–18 (2013).
29. Wrighton, K. C. et al. Fermentation, hydrogen, and sulfur metabolism in multiple uncultivated bacterial phyla. *Science* **337**, 1661–1665 (2012).
30. Parks, D. H. et al. Recovery of nearly 8,000 metagenome-assembled genomes substantially expands the tree of life. *Nat. Microbiol.* **2**, 1533–1542 (2017).
31. Castelle, C. et al. A new iron-oxidizing/O_2-reducing supercomplex spanning both inner and outer membranes, isolated from the extreme acidophile *Acidithiobacillus ferrooxidans*. *J. Biol. Chem.* **283**, 25803–25811 (2008).
32. Jeans, C. et al. Cytochrome 572 is a conspicuous membrane protein with iron oxidation activity purified directly from a natural acidophilic microbial community. *ISME J.* **2**, 542–550 (2008).
33. Croal, L. R., Jiao, Y. & Newman, D. K. The fox operon from *Rhodobacter* strain SW2 promotes phototrophic Fe(II) oxidation in *Rhodobacter capsulatus* SB1003. *J. Bacteriol.* **189**, 1774–1782 (2007).
34. Jiao, Y. & Newman, D. K. The *pio* operon is essential for phototrophic Fe(II) oxidation in *Rhodopseudomonas palustris* TIE-1. *J. Bacteriol.* **189**, 1765–1773 (2007).
35. He, S., Barco, R. A., Emerson, D. & Roden, E. E. Comparative genomic analysis of neutrophilic iron(II) oxidizer genomes for candidate genes in extracellular electron transfer. *Front. Microbiol.* **8**, 1584 (2017).
36. Richardson, D. J. et al. The 'porin-cytochrome' model for microbe-to-mineral electron transfer. *Mol. Microbiol.* **85**, 201–212 (2012).
37. Luther, G. W., III. Manganese(II) oxidation and Mn(IV) reduction in the environment—two one-electron transfer steps versus a single two-electron Step. *Geomicrobiol. J.* **22**, 195–203 (2005).
38. Lücker, S. et al. A *Nitrospira* metagenome illuminates the physiology and evolution of globally important nitrite-oxidizing bacteria. *Proc. Natl Acad. Sci. USA* **107**, 13479–13484 (2010).
39. Mundinger, A. B., Lawson, C. E., Jetten, M. S. M., Koch, H. & Lücker, S. Cultivation and transcriptional analysis of a canonical *Nitrospira* under stable growth conditions. *Front. Microbiol.* **10**, 1325 (2019).
40. Koch, H. et al. Growth of nitrite-oxidizing bacteria by aerobic hydrogen oxidation. *Science* **345**, 1052–1054 (2014).
41. Levicán, G., Ugalde, J. A., Ehrenfeld, N., Maass, A. & Parada, P. Comparative genomic analysis of carbon and nitrogen assimilation mechanisms in three indigenous bioleaching bacteria: predictions and validations. *BMC Genomics* **9**, 581 (2008).
42. Berg, I. A. Ecological aspects of the distribution of different autotrophic CO_2 fixation pathways. *Appl. Environ. Microbiol.* **77**, 1925–1936 (2011).
43. Thauer, R. K., Jungermann, K. & Decker, K. Energy conservation in chemotrophic anaerobic bacteria. *Bacteriol. Rev.* **41**, 100–180 (1977).
44. Baradaran, R., Berrisford, J. M., Minhas, G. S. & Sazanov, L. A. Crystal structure of the entire respiratory complex I. *Nature* **494**, 443–448 (2013).
45. Chadwick, G. L., Hemp, J., Fischer, W. W. & Orphan, V. J. Convergent evolution of unusual complex I homologs with increased proton pumping capacity: energetic and ecological implications. *ISME J.* **12**, 2668–2680 (2018).
46. Lücker, S., Nowka, B., Rattei, T., Spieck, E. & Daims, H. The genome of *Nitrospina gracilis* illuminates the metabolism and evolution of the major marine nitrite oxidizer. *Front. Microbiol.* **4**, 27 (2013).
47. Watson, S. W., Bock, E., Valois, F. W., Waterbury, J. B. & Schlosser, U. *Nitrospira marina* gen. nov. sp. nov.: a chemolithotrophic nitrite-oxidizing bacterium. *Arch. Microbiol.* **144**, 1–7 (1986).
48. Hippe, H. *Leptospirillum* gen. nov. (ex Markosyan 1972), nom. rev., including *Leptospirillum ferrooxidans* sp. nov. (ex Markosyan 1972), nom. rev. and *Leptospirillum thermoferrooxidans* sp. nov. (Golovacheva et al. 1992). Int. *J. Syst. Evol. Microbiol.* **50**, 501–503 (2000).
49. Henry, E. A. et al. Characterization of a new thermophilic sulfate-reducing bacterium *Thermodesulfovibrio yellowstonii*, gen. nov. and sp. nov.: its phylogenetic relationship to *Thermodesulfobacterium commune* and their origins deep within the bacterial domain. *Arch. Microbiol.* **161**, 62–69 (1994).
50. Lin, X., Kennedy, D., Fredrickson, J., Bjornstad, B. & Konopka, A. Vertical stratification of subsurface microbial community composition across geological formations at the Hanford site. *Environ. Microbiol.* **14**, 414–425 (2012).

Methods

No statistical methods were used to predetermine sample size. The experiments were not randomized and investigators were not blinded to allocation during experiments and outcome assessment.

Media and culture enrichment, refinement, and maintenance

A fortuitous enrichment culture for Mn(II) lithotrophs was established over the summer and autumn of 2015. A dense slurry of freshly precipitated $MnCO_3$ (see below) was distributed onto the internal surface of a wide-mouth glass jar and this coating was allowed to dry. The jar was filled completely with unsterilized Pasadena (California, USA) municipal drinking water (typically a blend from surface and aquifer sources) collected and allowed to stand for approximately 10 weeks, open and without agitation in an unoccupied room maintained at about 21 °C (co-ordinates: 34.1367°, −118.1273°). Additional freshly precipitated $MnCO_3$ was added as a dense suspension after the cream-coloured coating had blackened, and the jar was covered with a loose-fitting lid and allowed to incubate for several more months, after which a small amount (about 5% v/v) of the dark product was used to inoculate flasks of $MnCO_3$ suspended in municipal tap water. After this, a separate line of cultures was initiated in a defined, deionized water medium incubated in the laboratory at 37 °C.

The basal medium used for routine growth and maintenance of this line and in related experiments was adapted and modified from prior formulations[51,52]. The medium contained, per litre deionized H_2O: NaCl, 1 g; $MgCl_2{\cdot}6H_2O$, 400 mg; $CaCl_2{\cdot}2H_2O$, 1 g; KCl, 5 g; Na_2SO_4, 142 mg; $FeCl_3{\cdot}6H_2O$, 2 mg; H_3BO_3, 30 µg; $MnCl_2{\cdot}4H_2O$, 100 µg; $CoCl_2{\cdot}6H_2O$, 190 µg; $NiCl_2{\cdot}6H_2O$, 24 µg; $CuCl_2{\cdot}2H_2O$, 2 µg; $ZnCl_2$, 68 µg; Na_2SeO_3, 4 µg; Na_2MoO_4, 31 µg; riboflavin, 100 µg; biotin, 30 µg; thiamine HCl, 100 µg; L-ascorbic acid, 100 µg; d-Ca-pantothenate, 100 µg; folic acid, 100 µg; nicotinic acid, 100 µg; niacinamide, 100 µg; 4-aminobenzoic acid, 100 µg; pyridoxine HCl, 100 µg; lipoic acid, 100 µg; NAD, 100 µg; thiamine pyrophosphate, 100 µg; cyanocobalamin, 10 µg. As P source, a solution of potassium phosphate (pH 7.2) was added to a final concentration of 0.15 mM. As a nitrogen source, $NaNO_3$ was added to a final concentration of 1 mM; alternatively, 1 mM NH_4Cl or other nitrogen sources were used as noted. MOPS at its pK_a was added as a buffer to a final concentration of 5 mM, when noted. $MnCO_3$, or an alternative, heat-stable substrate for growth was added to the basal medium before steam sterilization; alternatively, heat-unstable substrate for growth was added using filter-sterilized stock solutions after the medium had adequately cooled.

Freshly precipitated $MnCO_3$ was used for the initial enrichment culture, for routine Mn(II)-dependent cultures in small volumes, for the serial dilution-to-extinction resolution of complex cultures, and for stock and starter cultures. To prepare this, 25 g $MnCl_2$ (Sigma-Aldrich no. 221279) was dissolved into 100 ml deionized water, yielding 125 ml of a 1.59 M $MnCl_2$ solution. Over the course of several minutes, this solution was slowly poured into 3 l of 0.33 M $NaHCO_3$ while vigorously stirring. After the cessation of stirring, the resultant precipitate was allowed to settle by gravity for about 1 h. Thereafter, the overlying reaction fluid was decanted and discarded. The precipitate was resuspended in 3 l of deionized water, and the stirring, settling, decanting and resuspension steps were repeated at least 10 times. After the final wash, the precipitate was resuspended in deionized water to a final volume of 100 ml, stored in a clean glass bottle, and refrigerated at 4 °C in the dark. Initially, the precipitate appeared white to light pink, but aged to a light tan within around 24 h. Thereafter, the material remained stable for months to years. Alternatively, a hydrated $MnCO_3$ substrate (Sigma-Aldrich no. 63539) was used for larger culture volumes, and/or for reproducible mass balances, as noted.

Cells were typically cultured in 10 ml of medium in 18-mm-diameter culture tubes, or in 100 ml of medium in 250-ml Erlenmeyer flasks at 37 °C, with 25 to 200 mM $MnCO_3$, as noted. To prevent dehydration of cultures over the long periods of incubation, cut strips of Parafilm (Heathrow Scientific) were used to seal the bottom edge of the 18-mm plastic test tube enclosures. Cultures were incubated stationary without agitation, or with shaking at 200 rpm, as noted.

To refine the number of species in the complex manganese-oxidizing enrichment, 5 successive rounds of serial tenfold dilution-to-extinction series were performed using 9 ml of $MnCO_3$ nitrate basal medium in 18-mm culture tubes, incubated at 32 °C. Culture tubes in each dilution series were scored as positive for the presence of lithotrophic manganese oxidizers when, after 2–12 weeks of incubation, the small and easily dispersed particles of the $MnCO_3$ substrate (light cream in colour) were converted to larger Mn oxide nodules or a single continuous Mn oxide coating (dark brownish-black in colour) that typically tightly adhered to the bottom of the glass culture tubes. Mn oxides from the final dilution tube showing such oxidation were used as the inocula for the next serial-dilution-to-extinction series.

To examine whether Mn(II) oxidation in the cultures was biological in nature, an active co-culture with Mn oxides was used to inoculate 18-mm culture tubes containing the basal medium with 50 mM $MnCO_3$. Cultures were amended with either of two antibiotics, kanamycin (30 µg/ml) or vancomycin (20 µg/ml), or pasteurized overnight at 50 °C before incubation at 32 °C. To examine the effect of incubation temperature on oxidation, cultures were incubated without agitation in different incubators set at a diversity of temperatures; incubation temperatures were regularly and independently confirmed with >2 thermometers. After 2 weeks, 2 ml mixtures from the cultures were sampled and stored at −80 °C for later inductively coupled plasma mass spectrometry (ICP-MS) analysis (see 'Chemical analysis of Mn'). Reported values were corrected for Mn oxides carried over in the inoculum, as ascertained by the lowest amount determined in the 50-°C pasteurization experiments.

To examine the growth of the culture in the absence of Mn(II) substrate, a stationary co-culture (confirmed separately to be viable) was used to inoculate 4 replicates of 250-ml Erlenmeyer flasks containing 120 ml of the basal medium without $MnCO_3$. The flasks were incubated at 37 °C with shaking at 200 rpm. After inoculation and after 10 and 21 days, 20 ml mixture from the cultures were sampled and centrifuged at 5,250*g* for 10 min; the pellet was stored at −80 °C. DNA was extracted from the thawed pellets using the DNeasy PowerSoil kit (Qiagen) following the manufacturer's instructions, with the bead beating option using FastPrep FP120 (Thermo Electron) at setting 5.5 for 45 s instead of the 10-min vortex step. DNA concentration was quantified using Qubit dsDNA High Sensitivity Assay Kit (Thermo Fisher Scientific).

To examine whether $MnCl_2$ can be oxidized by, or otherwise affects, growth: an active co-culture, which had oxidized 38% of the 35 mM $MnCO_3$ initially provided (measured using the ICP-MS method), was used to inoculate (10% v/v) 18-mm culture tubes containing 10 ml of the basal medium with 0.5–20 mM $MnCl_2$ instead of $MnCO_3$. After inoculation, and after days 5 and 10, 0.5 ml of the oxides and culture fluid mixture was sampled and stored at −80 °C for later ICP-MS analysis (see 'Chemical analysis of Mn'). Reported values were corrected for Mn oxides carried over in the inoculum, as ascertained by the lowest amount determined in the 0.5 mM $MnCl_2$ culture.

For attempts to observe single colony formation by Mn(II) lithotrophs on agar medium, the basal medium was adjusted to contain 200 mM $MnCO_3$ and 1.5% washed agar (BD Difco), and distributed into Petri dishes after steam sterilization.

Genomics predicts that each species in the co-culture may be able to produce compatible solutes (for example, trehalose and hydroxyectoine, by species A), and thus may be able to grow under a range of salinities. To examine the effect of increased salinity on the Mn(II)-oxidizing lithotrophs, the basal medium was amended with NaCl to achieve final salt concentrations of 2 ppt, 2.8 ppt, 3.8 ppt, 4.6 ppt, 5.5 ppt, 9 ppt, 16 ppt, 23 ppt, 30 ppt and 37 ppt (equivalent to 6%, 8%, 11%, 13%, 16%, 26%, 45%, 65%, 85% and 105% of the salinity of seawater, respectively).

After inoculation, oxidation in the tubes was monitored visually over time.

For isolation and maintenance of strains of species B (*Ramlibacter lithotrophicus*) from the co-culture (Supplementary Note 2), plates of agar-solidified (1.5% agar w/v, BD Life Sciences) basal medium were used except that sodium succinate (10 mM, final concentration) or tryptone (0.5% w/v, BD Life Sciences) were used in place of $MnCO_3$. Viable cells of this bacterium could rarely be retrieved from the co-culture as planktonic cells overlying Mn oxide nodules. For clonal isolation, 200 µl of a dense suspension of the dark Mn oxides produced by the co-culture were spotted onto the surface of succinate agar medium and allowed to dry, after which the Mn oxides were vigorously and heavily streaked over the agar surface and monitored for the development of colonies thereafter. After 3–5 days of incubation, colonies of species B appeared small, leathery and adherent to the agar surface; transfer of cells to new plates or liquid medium was facilitated by the use of a sterile syringe needle for the removal of an entire single colony from the agar surface. In liquid, newly isolated strains of species B can be grown with tryptone (0.5% w/v) or acetate (10 mM, final concentration) (Extended Data Fig. 6c, d), and can form fabric-like biofilms blanketing at the bottom of culture tubes. Transfer of such material proved challenging, as the fabric-like biomass typically adhered to the insides of both plastic and glass pipette surfaces, leading to the rapid selection for strain variants that do not form flocs.

For the examination of anaerobic growth of species B, 10 ml of basal medium was dispensed into 18-mm glass Balch tubes (Bellco) and stoppered with 1-cm butyl rubber stoppers under an N_2 headspace. Autotrophic growth of the isolate using $H_2 + O_2 + CO_2$ was examined similarly, except that an air headspace, periodically spiked with 1 ml of $H_2 + CO_2$ (80%/20%, v/v), was used. Colonies of species B did not develop on standard lysogen broth (LB) agar, or on plates of the basal medium amended with 5 g/l yeast extract (BD Biosciences), traits that were used to monitor for culture purity or contamination.

For growth of manganese-oxidizing lithotrophs in agarose tubes, the basal medium was amended to contain 150 mM freshly prepared $MnCO_3$ and 0.38% w/v agarose (Aquapor LE Ultrapure; National Diagnostics). After steam sterilization, 15-ml aliquots of the molten agar medium was dispensed into sterile 18-mm glass culture tubes fitted with plastic caps. After cooling to 45 °C in a water bath, the molten agar was inoculated with 0.5 ml of a dense suspension of Mn oxides from an actively growing lithotrophic culture, gently vortexed and allowed to harden on ice before incubation at 37 °C. Tubes were sealed with parafilm to avoid desiccation over the long periods of incubation, and monitored for both clearing of $MnCO_3$ as well as formation (or changes in the size, shape and distribution) of Mn oxide nodules.

Examination of Mn oxide nodules

In all the cases we examined, the generation of the dark, granular product was coincident with the generation of Mn oxides from Mn(II) CO_3, as determined via colourimetry[53], ATR-FTIR, reactivity with H_2O_2 and/or ICP-MS (see 'Chemical analysis of Mn').

To visualize, with minimal disturbance, cells on Mn oxide nodules generated in agarose tubes, cores of regions where the carbonate cleared and nodules developed were sampled with sterile glass Pasteur pipettes. Agar cores containing undisrupted nodules were extruded carefully into a plastic weigh boat and soaked in the basal medium (without $MnCO_3$) amended to contain 10 µg/µl acridine orange[54] for 30 min. The dye solution was decanted, and the core was soaked for 30 min in buffered medium without dye. The core was carefully transferred to glass microscope slides and gently covered with coverslips before examination via light microscopy. Light microscopy of Mn oxide nodules in agarose cultures was performed using both a Zeiss Stemmi 2000-C stereomicroscope and a Zeiss Axioplan 2 Imaging Microscope fitted with a HBO 100 mercury arc lamp housing and an ebq 100 lamp power supply (Lighting & Electronics Jena). For epifluorescence microscopy of acridine orange stained nodules, a blue (FITC) long-pass filter set was used (excitation, filter D470/40 Lot 33820 (Chroma Technology); emission, long-pass filter OG515 (515 nm cut-on; Schott)). Photodocumentation was with Panasonic Lumix GH3 and G85 microfourthirds-lens-mount cameras, mounted onto the research microscope via a combination of Zeiss to c-mount (1.0 X D10ZNC; Diagnostic Instruments) and 'c-mount to microfourthirds-mount' (Fotodiox) adaptors. RAW images were imported into Lightroom 9 (Adobe). Global adjustments to RAW images were made in Lightroom, for example, to improve clarity through the opaque agarose. The global changes to RAW images in this line of experiments involved correction for white balance and adjustments via the texture, clarity, dehazing, sharpening and 'colour-noise reduction' sliders.

For mineralogical analyses, Mn oxide nodules were collected from cultures and allowed to settle by gravity, washed three times with distilled water, incubated in consumer-grade concentrated bleach for 2 h at room temperature (to remove cellular and other organic carbon), washed three times with distilled water and then dried at 80 °C. Spectroscopic analyses were performed on Nicolet Magna 860 FTIR spectrophotometer (Thermo Nicolet) with attenuated total reflectance (ATR) accessory (Durascope, SensIR Technologies), and Nicolet iS50 FTIR spectrophotometer (Thermo Nicolet) with GladiATR ATR accessory (Pike Technologies).

For scanning electron microscopy (SEM) of the Mn oxide nodules, samples were chemically fixed on ice for 3–4 h in the basal medium amended with 2.5% glutaraldehyde and HEPES (25 mM, pH 7.5). Fixed samples were washed twice in the same buffered solution but without glutaraldehyde, and the final pellet was resuspended in the buffered solution with 50% (v/v) ethanol. Dehydration series were performed by increasing the ethanol concentration every 15 min to 70, 90 and finally 100% (v/v). Critical point drying (Quorum Technologies) was performed as follows: ethanol was replaced by liquid CO_2 at a pressure of 55 bar at <10 °C. Fifteen minutes after reaching the critical point, the pressure was released slowly at >35 °C until ambient pressure was reached. The samples were then deposited onto double coated carbon conductive tape (Ted Pella), and in some cases, were sputter coated with 10 nm of Pt/Pd (80/20 by weight, Cressington). SEM was performed using a field emission SEM (1550VP, Zeiss) with SE2 detector at an operating voltage of 10 kV.

Community analysis

An iTag 16S rRNA gene sequencing approach was used to obtain microbial community profiles. For such, a 2-ml culture sample containing Mn oxide nodules was centrifuged at 6,000*g* for 5 min. DNA was extracted from the pellets and quantified as described in 'Media and culture enrichment, refinement, and maintenance'. The V4–V5 region of the 16S rRNA genes was amplified using primers 515F-Y (5′-GTG YCA GCM GCC GCG GTA A-3′) and 926R (5′-GGA CTA CNV GGG TWT CTA AT-3′)[55] with Illumina adaptor overhangs[56] added to the oligonucleotides. PCR amplification was performed using 7.5 µl of Q5 High Fidelity 2X Master Mix (New England Biolabs), 0.75 µl of each forward and reverse primers (10 µM), 5 µl of PCR-grade water and 1 µl of DNA with a concentration about 1 ng/µl. PCR cycling condition was as following: initial denaturation at 98 °C for 2 min, 25 cycles of 98 °C for 10 s, 54 °C for 20 s, 72 °C for 20 s and a final extension of 72 °C for 2 min before cooling down to 6 °C. Duplicate PCR reactions for each samples were run; after confirming successful and comparable amplification using gel electrophoresis, the duplicates were combined for Illumina Nextera XT barcoding[56] using PCR condition as described above except in 25 µl reaction volume and 10 cycles with annealing at 66 °C. Barcoded samples were quantified using QuantIT PicoGreen dsDNA Assay (Thermo Fisher Scientific) on the C1000 Thermal Cycler with CFX96 Real-Time System (Bio-Rad), combined in equal molar amounts, and purified with QIAquick PCR Purification Kit (Qiagen). Sequencing was performed on the MiSeq

platform (Illumina) with paired 250-bp reads after PhiX addition of 15–20% (Laragen).

Sequence data were processed using QIIME[57] v.1.8.0. Raw sequences were first joined and quality-trimmed using the default read pair joining and quality-trimming parameters. Processed sequences were clustered into de novo operational taxonomic units (OTUs) at 99% sequence identity using UCLUST[58] v.7.11.0.667, with the most abundant sequence picked as the representative sequence for each OTU. OTUs with only a single sequence ('singletons') were removed. Taxonomic identification for the representative sequences were done using SILVA[59] Ref NR 99 database release 119.

Cloning of near full-length 16S rRNA genes of species A and species B

Near full-length 16S rRNA genes were amplified and cloned from the co-culture. First, DNA was extracted as in 'Media and culture enrichment, refinement, and maintenance'. Second, the 16S rRNA gene was amplified using primers BACT27F (5′-AGA GTT TGA TYM TGG CTC-3′) and U1492R (5′-GGY TAC CTT GTT ACG ACT T-3′) modified from published versions[60]. PCR was performed using the Expand High Fidelity System (Roche Molecular Systems) with the following conditions: 2.5 µl of 10 × buffer, 0.35 µl of Taq polymerase, 0.55 µl of 10 mM dNTP, 0.50 µl of each forward and reverse primer, 18.6 µl of PCR-grade water and 2 µl of a DNA extract. The cycling condition was as following: 95 °C for 2 min, followed by 30 cycles of 94 °C for 15 s, annealing at 54 °C for 30 s and extension at 72 °C for 45 s, and a final extension step at 72 °C for 4 min before cooling down to 4 °C. Third, the PCR products were immediately purified using QIAquick PCR purification kit (Qiagen), ligated into pGem-T Easy Vector (Promega), and the resulting plasmid was transformed into JM209 competent *Escherichia coli* cells (Promega) following the manufacturer's instructions. Over 50 white colonies were observed on X-gal containing plates from 50 µl of transformed cells. Clones were grown overnight at 37 °C in LB medium with 10% glycerol and 0.1 mg/ml ampicillin following the manufacturer's instructions (Promega). Lastly, PCR was performed using the NEB Taq Polymerase kit (New England Biolabs) with the following conditions: 3.0 µl of 10 × buffer, 0.66 µl of dNTP, 0.30 µl of Taq polymerase, 0.60 µl of each M13 forward and reverse primers (10 µM), 0.30 µl of 10 µg/µl bovine serum albumin, 23.95 µl of PCR water and 0.60 µl of cells. The cycling conditions were the same as the cloning reaction described above. The PCR products were purified using Multiscreen HTS PCR 96-well plates (Millipore). Sanger sequencing was performed on the purified PCR products to confirm their sequence identities using both M13 forward and reverse primers (Laragen).

FISH

Three oligonucleotide probes were developed or tested in this study to visualize and differentiate cells representing species A and species B in Mn oxide nodules (Supplementary Note 3, Extended Data Fig. 10a–d). SILVA[59] Ref NR 99 database release 128 and the PT server function of ARB software[61] v.6.0.2 were used for the development. The species A oligonucleotide probe (NLT499: 5′-ACA GAG TTA GCC GTG GCT-3′) was developed and designed to target the 16S rRNA genes from members of the classes Leptospirillia, Thermodesulfovibrionia, as well as other uncultivated classes within the phylum Nitrospirota[62]. Two oligonucleotide probes were used to target members of the order Betaproteobacteriales, including species B. Previously, a probe (BETA359 or Beta1: 5′-CCC ATT GTC CAA AAT TCC CC-3′)[63,64] had been reported, but the optimal hybridization conditions were not. A second probe was designed for this study (BETA867: 5′-AGG CGG TCA ACT TCA CGC-3′). A previously developed probe that targets most all bacteria (EUB338: 5′-GCT GCC TCC CGT AGG AGT-3′)[65] was also used for FISH. All probes were double-labelled[66]: with Cy3 dye for NLT499, FITC dye for BETA359 and BETA867, and Cy5 dye for EUB338 (Integrated DNA Technologies).

The clone-FISH method[67] was used to evaluate the specificity and hybridization conditions of these three oligonucleotide probes. Transformed JM209 *E. coli* (see 'Cloning of near full-length 16S rRNA genes of species A and species B') containing either the 16S rRNA gene of species A or species B were grown overnight at 37 °C with shaking at 200 rpm in ampicillin-containing LB medium. Plasmids were isolated using the QIAprep Spin Miniprep Kit (Qiagen) following the manufacturer's instructions. Isolated plasmids were then transformed into NovaBlue(DE3) *E. coli* competent cells (EMD Millipore) following the manufacturer's instructions. 16S rRNA gene sequence of transformed NovaBlue(DE3) cells were confirmed as described in 'Cloning of near full-length 16S rRNA genes of species A and species B' by Sanger sequencing (Laragen). Cells for clone-FISH were prepared as previously described[67]. In brief, overnight cultures of optical density at 600 nm (OD_{600}) of about 0.4 were induced with IPTG (1 mM) for 2 h, and chloramphenicol (170 mg l^{-1}) was added to the cultures and incubated for 5 h. The cells were then collected by centrifuging at 8,000*g* for 10 min, fixed with 4% paraformaldehyde in 1× PBS, washed twice with PBS and stored in PBS:ethanol (1:1) at −20 °C. FISH reactions were performed as previously described[68] prior to epifluorescence microscopy using a BX51 epifluorescence microscope (Olympus) with 100× (UPlanFL N) oil immersion objective. Each point in the dissociation profile represents the mean of fluorescence intensities of at least 100 single cells in 5 microscopic fields evaluated using the software daime[69] v.2.1 with default automatic segmentation settings of the threshold algorithm Isodata, and manually size-filtering resulting regions of interest for single-cell analysis.

To prepare Mn oxide nodules for FISH visualization, Superfrost Micro Slide (VWR Scientific) were dipped in 0.2% UltraPure agarose (Thermo Fisher Scientific) at 45 °C. Mn oxide nodules were fixed with paraformaldehyde as above, except stored in PBS at 4 °C for no longer than 2 weeks. Fixed Mn oxide nodules in PBS were immediately pipetted onto the warm slide and cooled to room temperature. After this, the slide was dipped in freshly prepared DCBE buffer (0.05 M sodium dithionite, 0.1 M sodium citrate, 0.1 M sodium bicarbonate and 0.1 M EDTA at pH 7; a modification of DCB buffer[70]) for 5 min at room temperature to dissolve away the Mn, leaving nodule-associated cells constrained within the agarose. The cells were then permeabilized with protease K (15 µg/ml) for 10 min at room temperature, and lysozyme (10 mg/ml) for 30 min at 37 °C. The slide was washed once in 0.01 M HCl for 15 min and three times in water for 1 min each before drying at 37 °C. The permeabilization and HCl washing is not necessary for FISH reactions to work, and can be omitted. FISH reactions, using NLT499-Cy3, BETA867-FITC and EUB338-Cy5 probes, were performed in 35% formamide hybridization buffer[68] with corresponding salt concentration in the washing buffer[68]. DAPI–citifluor (5 µg/ml) was added to the FISH samples before epifluorescence microscopy using a BX51 epifluorescence microscope (Olympus) with 100× (UPlanFL N) oil immersion objective.

Stable isotope probing and nanoSIMS analyses

Mn-oxidizing co-cultures were grown in basal medium containing $Mn^{13}CO_3$ and $^{15}NO_3^-$ to visualize the assimilation of ^{13}C and ^{15}N into the cells of species A and species B. For these, 0.5-ml samples from a stationary culture grown in basal medium with 26 mM unlabelled $MnCO_3$ was transferred into 18-mm glass Balch tubes containing 9.6 ml of autoclaved basal medium with 13 mM $Mn^{13}CO_3$ (prepared using ^{13}C-$NaHCO_3$, 99 atom % ^{13}C, Cambridge Isotope Laboratories). For a nitrogen source, the medium contained 1 mM $Na^{15}NO_3$ (98 atom % ^{15}N, Sigma-Aldrich Isotec, no. 364606). The culture tubes were stoppered under about 20 ml of air headspace with 1-cm butyl rubber stoppers, and incubated at 37 °C without shaking until, by visual examination, no $MnCO_3$ appeared to remain. Resulting Mn oxide nodules were fixed with paraformaldehyde, dissolved with DCBE buffer (see 'FISH') by shaking at 37 °C for 1 h, and filtered onto 0.20-µm polycarbonate filters (Isopore GTBP02500, Millipore) that have been sputter coated

with 10 nm of Au. FISH reactions were performed on the filters (as described in 'FISH' but without permeabilization and HCl washing) in 25% formamide hybridization buffer. As evaluated in Clone-FISH, no probe cross-reaction was observed in the 25% formamide hybridization buffer used to increase signal intensity. A culture grown in the presence of 13 mM unlabelled $MnCO_3$ (prepared using $NaHCO_3$, Thermo Fisher Scientific, no. S233-500) and 1 mM $Na^{15}NO_3$ was used for comparison and as a control. DAPI–citifluor (5 μg/ml) was added to the FISH samples before epifluorescence microscopy using a Elyra S1 (Zeiss) fitted with a Plan-Apochromat 63×/1.4 Oil immersion DIC objective. In parallel, to both assess and to minimize the dilution of the ^{13}C and ^{15}N signal in labelled biomass (for example, by some unlabelled reagents such as paraformaldehyde and reagents for FISH) during post-incubation sample preparations: Mn oxide nodules were dissolved as described in 'FISH' with DCBE buffer but without paraformaldehyde fixation, with the resultant cells subsequently stained for epifluorescence microscopy with DAPI–citifluor only (that is, no FISH reagents). However, the dissolution of nodules for analyses required the use of DCBE buffer which contains unlabelled citric acid, bicarbonate and EDTA, residuum from which, if associated with biomass from the nodules, would artefactually lower estimates of the extent of the labelling, especially for ^{13}C. Finally, filters were washed in ethanol with increasing concentrations (50%, 80% and 100%) each for 3 min before mounting on nanoSIMS holder using double coated carbon conductive tape (Ted Pella).

NanoSIMS analysis was performed using a CAMECA NanoSIMS 50L at the Caltech Microanalysis Center. A focused primary Cs^+ beam of 100–1,000 pA was used for pre-sputtering the sample until $^{12}C^{14}N^-$ counts stabilized, and 2–4 pA was used for image collection with rasters of 512 × 512 pixels. Secondary ions $^{12}C^{12}C^-$, $^{13}C^{12}C^-$, $^{12}C^{14}N^-$, $^{12}C^{15}N^-$ and $^{32}S^-$ were measured simultaneously for at least 3 image frames. In one instance, a region was measured a second time with $^{55}Mn^{16}O^-$ added to the analysis to confirm the absence of Mn in the sample. Individual ion image frames in the resulting data were aligned using the $^{12}C^{14}N^-$ ion, and then epifluorescence microscopy images were transformed to match that of nanoSIMS ion images using Look@NanoSIMS[71] v.2019-05-14; regions of interest (ROIs) corresponding to cells of species A or species B were defined manually. Final ion counts per ROI were calculated by summation of ion counts over all image frames. Atom per cent of ^{13}C or ^{15}N was calculated from the individual ion counts as described in Supplementary Note 9.

Kinetics of Mn(II) oxidation and cell growth

Glassware used in the kinetic experiments was acid-washed with 3.7% HCl and combusted at 550 °C to eliminate residue metals and organic carbon. All cultures were incubated at 37 °C with shaking at 200 rpm.

The kinetic experiments were performed in 1-l flasks with 0.4 l of the basal medium using commercial $MnCO_3$ (Sigma-Aldrich) with a final content of 100 mM Mn(II) as determined using the ICP-MS method (see 'Chemical analysis of Mn'). The basal media contain either 1 mM $NaNO_3$ ($n = 4$) or 1 mM NH_4Cl ($n = 5$) as the nitrogen source. Each culture flask was inoculated with 5 ml of a Mn oxide slurry sampled from a flask of an active co-culture grown with 1 mM nitrate and 1 mM urea as the nitrogen source. Culture material was sampled from each flask daily for the first 36 days, followed by 3 final, well-separated time points over the final 30 days. At each time point, culture flasks were removed from the shaking incubator and swirled. Immediately thereafter, a total of 3 ml of oxides and culture fluid mixture was aseptically sampled from the flask via a 5-ml disposable pipette. Of this, 1 ml of the sample was saved at −80 °C for later ICP-MS analysis (see 'Chemical analysis of Mn'); 2 ml of the sample was centrifuged at 8,000*g* for 5 min and the pellet was stored at −80 °C for later quantitative PCR analyses. DNA was extracted from the pellets and quantified as described in 'Media and culture enrichment, refinement, and maintenance'.

Chemical analysis of Mn

Reduced Mn(II) and oxidized manganese (a combination of Mn(III) and Mn(IV)) pools were measured using a previously described method[6] and evaluated (Supplementary Note 4, Extended Data Fig. 10e). In brief, 0.1 ml of oxide and culture fluid mixture was mixed with 0.9 ml of 0.5 N HCl. After reacting for at least 10 min, the mixture was centrifuged at 16,100*g* for 3 min. The supernatant (acid-soluble fraction, representing Mn(II)) was pipetted out into a separate tube. The pellet (acid-insoluble fraction, representing Mn(III) and Mn(IV)) was then reacted with 1 ml of 0.25 N $NH_2OH{\cdot}HCl$ in 0.25 N HCl. The acid-soluble and acid-insoluble fractions were then centrifuged again at 16,100*g* for 3 min to avoid any carryover. From each fraction, 0.1 ml was sampled and then diluted into 10 ml of 2% HNO_3. The Mn contents were measured using an Agilent 8800 inductively coupled plasma mass spectrometer (Agilent Technologies) with the helium gas collision mode and quantified using a Mn standard solution (Sigma-Aldrich, Supelco 1.19789). Attempts were also made to measure total Mn content using the formaldoxime method[72], and oxidized Mn(III) and Mn(IV) content using the leucoberbelin blue dye[53,73]. However, both methods resulted in underestimates of the manganese content when compared to the ICP-MS method and standards. In large part, this was due to the relatively large Mn oxide nodules being challenging to both dissolve and to react with those reagents to completion.

For determining dissolved Mn concentrations in particle-free fluids associated with $MnCO_3$ and spent cultures, fluids were sampled from uninoculated and inoculated cultures containing 20–100 mM $MnCO_3$. From each sample, 0.1 ml was subsampled after centrifuging at 16,000*g* for 3 min, subsequently filtered through a 0.22-μm filter, and each fraction dissolved into 10 ml of 2% HNO_3. The ICP-MS measurements for Mn(II) and the combined Mn(III) and Mn(IV) fractions were performed as described above.

Quantitative PCR

To obtain standards and test quantitative PCR specificity, plasmids with 16S rRNA gene of either species A or species B were purified from transformed JM209 *E. coli* as described in 'FISH'. Purified plasmids were then linearized using 150 units of restriction enzyme SacI in 50-μl reactions containing 1 × NEB Buffer 1 (New England Biolabs) overnight at 37 °C. The restriction digest reactions were heat-inactivated at 65 °C for 20 min and purified using Multiscreen HTS PCR 96-well plates (Millipore). Concentration of the linearized and purified plasmids were quantified using the Qubit dsDNA HS Assay Kit (Thermo Fisher Scientific) to make DNA template standards containing known copies of 16S rRNA genes of species A or species B.

To track the growth of all bacteria in Mn-oxidizing cultures, quantitative PCR assays were performed based on an assay developed and optimized previously[74] (Supplementary Note 5, Extended Data Fig. 10g–j). All primers and probes were obtained from Integrated DNA Technologies and diluted in 10 mM Tris·HCl (pH 8.0). The forward and reverse primers used, BACT1369F1 (5′-CGG TGA ATA CGT TCC CGG-3′) and PROK1492R1 (5′-GGC TAC CTT GTT ACG ACT T-3′), were one version of the previous degenerate primers BACT1369F and PROK1492R. The TaqMan probe for prokaryotes, TM1389F (TM1389F-FAM-ZEN, 5′-CTT GTA CAC ACC GCC CGT C-3′), was modified on the 5′ with 6-FAM fluorophore, 3′ with Iowa Black FQ dark quencher and internally with ZEN quencher. Also, TaqMan probes that specifically target species A and species B were developed. The specific species A TaqMan probe TM1484R-A (5′-ATC ACC AAT CAT ACC TTG GGT GCC TG-3′) was modified on the 5′ with HEX fluorophore, 3′ with Iowa Black FQ dark quencher and internally with ZEN quencher. The specific species B TaqMan probe TM1484R-B (5′-GTC ACG AAC CCT GCC GTG GTA ATC-3′) was modified at the 5′ with Texas Red-X fluorophore and 3′ with Iowa Black RQ dark quencher. Optimized quantitative PCR reaction mixtures contain 10 μl of PrimeTime Gene Expression Master Mix (Integrated DNA

Technologies), 1 µl of each forward and reverse primer (10 µM), 0.5 µl of each of the three TaqMan probes, 5.5 µl of PCR-grade water, and 1 µl of template DNA. The reactions were run in triplicates at 95 °C for 3 min, followed by 40 cycles of 95 °C for 10 s and 62 °C for 30 s, on the C1000 Thermal Cycler with CFX96 Real-Time System (Bio-Rad). The amplification efficiency was calculated as amplification efficiency = $10^{(-1/\text{slope})} - 1$. The upper and lower limits of quantification ranges were determined based on dilution of standards with amplification efficiencies in the log-linear phase between 90–105%. To convert to cell number, the 16S rRNA gene copies quantified in quantitative PCR assays were divided by 1 or 2 for species A or species B, respectively, based on the number of 16S rRNA gene copy number per genome.

Genomics

To obtain genomic DNA from species B, a flask with 200 ml of the basal medium containing 5 g/l of both tryptone and yeast extract was inoculated with a single colony of isolated species B from a succinate nitrate medium plate. The culture was grown at 37 °C with shaking at 200 rpm until early stationary phase, then collected by centrifuging at 5,250*g* for 30 min at room temperature. DNA from the cell pellets was extracted following the bacterial genomic DNA isolation using CTAB protocol version 3 as previously described[75]. Ethanol-precipitated DNA was additionally purified using the PureLink PCR Purification Kit (Thermo Fisher Scientific) following the manufacturer's instructions. To obtain genomic DNA from the co-culture, Mn oxide nodules were collected from an early stationary phase culture: 2 ml of culture containing about 0.15 g of Mn oxide nodules was centrifuged at 5,000*g* for 10 min at room temperature. DNA was extracted from the pellet using the DNeasy PowerSoil kit (Qiagen) as described in 'Media and culture enrichment, refinement, and maintenance'. DNA extract was purified and concentrated using protocol A of the CleanAll DNA/RNA Clean-up and Concentration Micro Kit (Norgen Biotek) following the manufacturer's instructions.

Purified genomic DNA samples (2–50 ng) were fragmented to the average size of 600 bp via use of a Qsonica Q800R sonicator (power: 20%; pulse: 15 s on/15 s off; sonication time: 3 min). Libraries were constructed using the NEBNext Ultra II DNA Library Prep Kit (New England Biolabs) following the manufacturer's instructions. In brief, fragmented DNA was end-repaired using a combination of T4 DNA polymerase, *E. coli* DNA Pol I large fragment (Klenow polymerase) and T4 polynucleotide kinase. The blunt, phosphorylated ends were treated with Klenow fragment (3′ to 5′ exo minus) and dATP to yield a protruding 3′ 'A' base for ligation of NEBNext Multiplex Oligos for Illumina (New England Biolabs) which have a single 3′ overhanging T base and a hairpin structure. After ligation, adapters were converted to the Y shape by treating with USER enzyme and DNA fragments were size selected using Agencourt AMPure XP beads (Beckman Coulter) to generate fragment sizes between 500 and 700 bp. Adaptor-ligated DNA was PCR-amplified with 8 to 12 cycles depending on the input amount followed by AMPure XP bead clean up. Libraries were quantified with Qubit dsDNA HS Kit (Thermo Fisher Scientific) and the size distribution was confirmed with High Sensitivity DNA Kit for Bioanalyzer (Agilent Technologies). Sequencing was performed on HiSeq2500 platform (Illumina) with paired 250-bp reads following the manufacturer's instructions. Base calls were performed with RTA v.1.18.64 followed by conversion to FASTQ with bcl2fastq v.1.8.4 (Illumina). In addition, reads that did not pass the Illumina chastity filter as identified by the Y flag in their fastq headers were discarded. The resulting reads were uploaded to the KBase platform[76], trimmed using Trimmomatic[77] v.0.36 with default settings and adaptor clipping profile Truseq3-PE, and assembled using Spades[78] v.3.11.1 with default settings for standard dataset. Manual binning and scaffolding were performed using mmgenome v.0.7.1[79], using differential coverage from isolated species B versus the species A + species B co-culture, to generate genome bins for species A and species B. Trimmed reads were aligned to either the species A or species B genome bin using bowtie2[80] v.2.3.4.1 with default settings. Finally, the resulting reads were reassembled using Spades[78] v.3.11.1 with --careful setting and manually binned with mmgenome[79] v.0.7.1 once again, excluding contigs <500 bp. Reconstructed genomes were annotated using the IMG[81] Microbial Genome Annotation and the National Center for Biotechnology Information (NCBI)[82] Prokaryotic Genome Annotation Pipelines; β-barrel protein prediction was performed using PRED-TMBB[83].

Phylogenetic analyses

For species A phylogenies, 275 publicly available genome assemblies in NCBI assembly database[82] (as of 26 March 2019) were analysed. These fell within the phylum Nitrospirae (taxonomy identifier 40117)[84], which corresponded to the phylum under the headings 'Nitrospirota' and 'Nitrospirota_A' in the Genome Taxonomy Database (GTDB)[62] v.0.2.2. Genome assemblies with estimated completeness of <60% and contamination of >5% (based on CheckM[85] v.1.0.6) were excluded. For 16S rRNA gene phylogeny, 16 s rRNA genes from the genome of species A or species B, as well as the genome assemblies, were retrieved using CheckM[85] v.1.0.6 ssu_finder utility. Sequences of less than 900 bp and containing more than 2 N were excluded. The 16S rRNA gene sequences were aligned using SINA[86] v.1.2.11 and imported into SILVA[59] Ref NR 99 database release 128. Sixty 16S rRNA gene sequences, including 5 different outgroup sequences (*Desulfovibrio vulgaris*, *Ramlibacter tataouinensis* TTB310, *Nitrospina gracilis* 3/211, *Acidobacterium capsulatum* and '*Candidatus* Methylomirabilis oxyfera'), with 1,532 nucleotide positions were exported with bacteria filter in the SILVA database. Bayesian phylogenetic trees were constructed using MrBayes[87] v.3.2.6 with evolutionary model set to GTR + I + gamma, burn-in set to 25% and stop value set to 0.01, and edited in iTOL[88]. For concatenated multilocus protein phylogeny, marker proteins from 40 genomes including the same 5 outgroup species were identified and aligned using a set of 120 ubiquitous single-copy bacterial proteins in GTDB[62] v.0.2.2. The protein alignment was filtered using default parameters in GTDB[62] v.0.2.2 (the full alignment of 34,744 columns from 120 protein markers were evenly subsampled with a maximum of 42 columns retained per protein; a column was retained only when the column was in at least 50% of the sequences, and contained at least 25% and at most 95% of one amino acid). The resulting alignment with 5,036 amino acid positions was used to construct the multilocus protein phylogeny using MrBayes[87] v.3.2.6 as described above, except the evolutionary model was set to invgamma and a mixed amino acid model.

For species B phylogenies, 60 publicly available genome assemblies were selected from the NCBI assembly database[82] under the class Betaproteobacteria (taxonomy identifier 28216)[84], which corresponds to the order Betaproteobacteriales in GTDB[62] v.0.2.2. These 60 genomes assemblies had >93% completeness and <3% contamination based on CheckM[85] v.1.0.6, and represented different genera. The same 5 outgroups were used as for species A, except *Ramlibacter tataouinensis* TTB310 was replaced with *Nitrospira inopinata*. Bayesian 16S rRNA gene phylogeny was performed as described for species A with 1,532 aligned nucleoic acid positions. Maximum-likelihood multilocus protein phylogeny was constructed using 5,035 amino acid positions using RAxML[89] v.8.1.7 with protein model GAMMALGF and rapid bootstrapping of 100 replicates.

For functional gene phylogeny, protein sequences were aligned using ClustalO[90] v.1.2.4 and maximum likelihood trees were constructed using RAxML[89] v.8.1.7 with protein model GAMMALGF and rapid bootstrapping of 100 replicates.

Transcriptomics

Glassware treatment and culturing condition for the transcriptomics experiments were as described in 'Kinetics of Mn(II) oxidation and cell growth'. Three replicates from different, actively Mn-oxidizing cultures were used as inocula for RNA experiments. A 5% v/v inoculum

from two active Mn-oxidizing cultures was transferred into triplicate flasks containing the basal medium amended with 100 mM freshly prepared $MnCO_3$, for a total of 6 flasks (sample identifiers: Mn03/Mn06/Mn08 and Mn09/Mn10/Mn11). A 1% v/v inoculum from another active Mn-oxidizing culture was transferred into a 7th flask of the same medium (sample identifier Mn12). For collecting biomass before the complete oxidation of Mn(II) (Extended Data Fig. 3h), shaking of the incubator was paused for 3 min to allow Mn oxide nodules to settle by gravity. The overlaying medium was then decanted off until about 10 ml of culture and oxides remained. First 35 ml and then 15 ml of LifeGuard Soil Preservation Solution (Qiagen) was added, sequentially, to maximize transfer efficiency of Mn oxide nodules from the culture into a new 100-ml centrifuge tube. The culture–LifeGuard mixture was stored at 4 °C for less than a week, a duration for which RNA was expected to remain well-preserved, according to the manufacturer. Initially, a series of different trials were performed (using multiple methods and variations, including the RNeasy Mini Kit (Qiagen), the RNeasy Powersoil Kit (Qiagen), and a previous customized procedure[91]) to directly extract RNA from Mn oxide nodules. None of these extracted measurable RNA from samples. When an early chemical dissolution step was added, the extraction of RNA from Mn oxide nodules was successful in combination with the following procedures. Before RNA extraction: the culture–lifeguard mixture was first centrifuged at 5,250*g* for 10 min at 4 °C. Four hundred ml of freshly prepared 0.22-µm-filtered DCBE solution (for recipe, see 'FISH') was added to the pellet and incubated at 37 °C with shaking at 200 rpm for 10 min to dissolve the Mn oxide nodules. The dissolved samples were then centrifuged at 5,250*g* for 10 min at 4 °C. The supernatant was decanted, and the remaining 5 ml of material was mixed with 10 ml of 0.22-µm-filtered and autoclaved CBE solution (similar to the DCBE solution, but without sodium dithionite). The mixture was then centrifuged at 5,250*g* for 10 min at 4 °C. The supernatant was discarded, and 0.9 ml of RLT solution with 2-mercaptoethanol from the RNeasy Mini Kit (Qiagen) was added to the pellet. The mixture was transferred into glass 0.1-mm PowerBead Tubes (Qiagen) and bead-beat using FastPrep FP120 (Thermo Electron) at setting 5.5 for 45 s. RNA extraction then proceeded using the RNeasy Mini Kit (Qiagen) according to the manufacturer's instructions. DNA from the extracted RNA was removed using the DNase Max Kit (Qiagen). The RNA extracts were purified and concentrated using protocol C of the CleanAll DNA/RNA Clean-up and Concentration Micro Kit (Norgen Biotek) and stored at −80 °C until sequencing library preparation.

For RNA sequencing library preparation, RNA integrity was first assessed using RNA 6000 Pico Kit for Bioanalyzer (Agilent Technologies). RNA sequencing (RNA-seq) libraries were constructed using NEBNext Ultra II RNA Library Prep Kit for Illumina (New England Biolabs) following the manufacturer's instructions. In brief, 1–10 ng of total RNA was fragmented to the average size of 200 bp by incubating at 94 °C for 15 min in first-strand buffer, cDNA was synthesized using random primers and ProtoScript II Reverse Transcriptase followed by second-strand synthesis using NEB Second Strand Synthesis Enzyme Mix. Resulting DNA fragments were end-repaired, dA-tailed and ligated to NEBNext hairpin adaptors (New England Biolabs). After ligation, adaptors were converted to the Y shape by treating with USER enzyme and DNA fragments were size-selected using Agencourt AMPure XP beads (Beckman Coulter) to generate fragment sizes between 250 and 350 bp. Adaptor-ligated DNA was PCR-amplified followed by AMPure XP bead clean up. Libraries were quantified with Qubit dsDNA HS Kit (Thermo Fisher Scientific), and the fragments were determined to a mean of 350 bp with standard deviation of 70 bp using High Sensitivity DNA Kit for Bioanalyzer (Agilent Technologies). Sequencing was performed on the HiSeq2500 platform (Illumina) with single-end 50- and 100-bp reads following the manufacturer's instructions. Base calls were performed with RTA 1.18.64 followed by conversion to FASTQ with bcl2fastq 1.8.4 (Illumina). Low-quality reads and TruSeq3-SE adaptors were removed using Trimmomatic[77] v.0.36 with default settings. rRNA was removed using sortmerna[92] v.2.0 with supplied SILVA databases and default settings. Read mapping of the non-rRNA was performed using kallisto[93] v.0.44.0 with 100 bootstraps, fragment mean of 130 bp and standard deviation of 70 bp. The fragment mean was determined to be 230 bp using Agilent Bioanalyzer, after adaptor removal (120 bp), but this input parameter caused an issue in evaluating gene expression of genes smaller than 230 bp in kallisto[93] v.0.44.0. The fragment mean was therefore decreased while not affecting the overall transcript expression (Extended Data Fig. 10f). Final analysis and normalization of different RNA samples was performed using sleuth[94] v.0.30.0, with the reconstructed genomes of both species (Supplementary Tables 3, 5) or only of species A (Supplementary Table 4). Extended Data Fig. 3h includes RNA processing statistics of the processed files where read mapping was done using BBMap (https://sourceforge.net/projects/bbmap/) v.37.93 with minid = 0.97 ambiguous = toss settings.

Reporting summary

Further information on research design is available in the Nature Research Reporting Summary linked to this paper.

Data availability

All sequencing data has been deposited at the NCBI under BioProject PRJNA562312. The cloned 16S rRNA gene sequences of '*Candidatus* Manganitrophus noduliformans' (species A) and *R. lithotrophicus* (species B) from the co-culture have been deposited at GenBank under accession numbers MN381734 and MN381735, respectively. The iTAG sequences from the different enrichments have been deposited at the Sequence Read Archive (SRA) under accession numbers SRR10031198, SRR10031199 and SRR10031200. Genome sequences of the co-culture, from which the genome of '*Candidatus* Manganitrophus noduliformans' was reconstructed, have been deposited under BioSample SAMN12638105 with raw sequences deposited at SRA under accession number SRR10032644; the reconstructed genome of '*Candidatus* Manganitrophus noduliformans' has been deposited at DDBJ/ENA/GenBank under accession number VTOW00000000. Genome sequences of *R. lithotrophicus* strain RBP-1 have been deposited under BioSample SAMN12638106, with raw sequences deposited at SRA under accession number SRR10031379; the reconstructed genome of *R. lithotrophicus* strain RBP-1 has been deposited at DDBJ/ENA/GenBank under accession number VTOX00000000. Additionally, reconstructed genomes have been deposited in Joint Genome Institute (JGI) Genomes Online Database Study ID Gs0134339, with Integrated Microbial Genome ID 2784132095 for '*Candidatus* Manganitrophus noduliformans' and ID 2778260901 for *R. lithotrophicus* strain RBP-1. Transcriptome sequence data for the seven biological replicates have been deposited at SRA under accession numbers SRR10060009, SRR10060010, SRR10060011, SRR10060012, SRR10060013, SRR10060017 and SRR10060018. Unique biological materials are available from the corresponding author upon reasonable request. Source data are provided with this paper.

51. Flagan, S., Ching, W.-K. & Leadbetter, J. R. *Arthrobacter* strain VAI-A utilizes acyl-homoserine lactone inactivation products and stimulates quorum signal biodegradation by *Variovorax paradoxus*. *Appl. Environ. Microbiol.* **69**, 909–916 (2003).
52. Leadbetter, J. R. & Greenberg, E. P. Metabolism of acyl-homoserine lactone quorum-sensing signals by *Variovorax paradoxus*. *J. Bacteriol.* **182**, 6921–6926 (2000).
53. Krumbein, W. E. & Altmann, H. J. A new method for the detection and enumeration of manganese oxidizing and reducing microorganisms. *Helgol. Wiss. Meeresunters.* **25**, 347–356 (1973).
54. Emerson, D. & Revsbech, N. P. Investigation of an iron-oxidizing microbial mat community located near Aarhus, Denmark: laboratory studies. *Appl. Environ. Microbiol.* **60**, 4032–4038 (1994).
55. Parada, A. E., Needham, D. M. & Fuhrman, J. A. Every base matters: assessing small subunit rRNA primers for marine microbiomes with mock communities, time series and global field samples. *Environ. Microbiol.* **18**, 1403–1414 (2016).
56. Illumina. 16S Metagenomic sequencing library preparation, https://support.illumina.com/downloads/16s_metagenomic_sequencing_library_preparation.html (2013).

57. Caporaso, J. G. et al. QIIME allows analysis of high-throughput community sequencing data. *Nat. Methods* **7**, 335–336 (2010).
58. Edgar, R. C. Search and clustering orders of magnitude faster than BLAST. *Bioinformatics* **26**, 2460–2461 (2010).
59. Quast, C. et al. The SILVA ribosomal RNA gene database project: improved data processing and web-based tools. *Nucleic Acids Res*. **41**, D590–D596 (2013).
60. Lane, D. J. in *Nucleic Acid Techniques in Bacterial Systematics* (eds Stackebrandt, E. & Goodfellow, M.) 115–175 (John Wiley & Sons, 1991).
61. Ludwig, W. et al. ARB: a software environment for sequence data. *Nucleic Acids Res*. **32**, 1363–1371 (2004).
62. Parks, D. H. et al. A standardized bacterial taxonomy based on genome phylogeny substantially revises the tree of life. *Nat. Biotechnol*. **36**, 996–1004 (2018).
63. Schönmann, S. et al. 16S rRNA gene-based phylogenetic microarray for simultaneous identification of members of the genus *Burkholderia*. *Environ. Microbiol*. **11**, 779–800 (2009).
64. Greuter, D., Loy, A., Horn, M. & Rattei, T. probeBase—an online resource for rRNA-targeted oligonucleotide probes and primers: new features 2016. *Nucleic Acids Res*. **44**, D586–D589 (2016).
65. Amann, R. I. et al. Combination of 16S rRNA-targeted oligonucleotide probes with flow cytometry for analyzing mixed microbial populations. *Appl. Environ. Microbiol*. **56**, 1919–1925 (1990).
66. Stoecker, K., Dorninger, C., Daims, H. & Wagner, M. Double labeling of oligonucleotide probes for fluorescence *in situ* hybridization (DOPE-FISH) improves signal intensity and increases rRNA accessibility. *Appl. Environ. Microbiol*. **76**, 922–926 (2010).
67. Schramm, A., Fuchs, B. M., Nielsen, J. L., Tonolla, M. & Stahl, D. A. Fluorescence *in situ* hybridization of 16S rRNA gene clones (Clone-FISH) for probe validation and screening of clone libraries. *Environ. Microbiol*. **4**, 713–720 (2002).
68. Daims, H., Stoecker, K. & Wagner, M. in *Molecular Microbial Ecology* (eds Osborn, M. A. and Smith, C. J.) 208–228 (Taylor & Francis, 2004).
69. Daims, H., Lücker, S. & Wagner, M. daime, a novel image analysis program for microbial ecology and biofilm research. *Environ. Microbiol*. **8**, 200–213 (2006).
70. Taylor, G. J. & Crowder, A. A. Use of the DCB technique for extraction of hydrous iron oxides from roots of wetland plants. *Am. J. Bot*. **70**, 1254 (1983).
71. Polerecky, L. et al. Look@NanoSIMS—a tool for the analysis of nanoSIMS data in environmental microbiology. *Environ. Microbiol*. **14**, 1009–1023 (2012).
72. Brewer, P. G. & Spencer, D. W. Colorimetric determination of manganse in anoxic waters. *Limnol. Oceanogr*. **16**, 107–110 (1971).
73. Oldham, V. E., Miller, M. T., Jensen, L. T. & Luther, G. W. Revisiting Mn and Fe removal in humic rich estuaries. *Geochim. Cosmochim. Acta* **209**, 267–283 (2017).
74. Suzuki, M. T., Taylor, L. T. & DeLong, E. F. Quantitative analysis of small-subunit rRNA genes in mixed microbial populations via 5′-nuclease assays. *Appl. Environ. Microbiol*. **66**, 4605–4614 (2000).
75. William, S., Feil, H. & Copeland, A. Bacterial genomic DNA isolation using CTAB, Department of Energy Joint Genome Institute, https://jgi.doe.gov/user-programs/pmo-overview/protocols-sample-preparation-information/ (2012).
76. Arkin, A. P. et al. KBase: the United States Department of Energy systems biology knowledgebase. *Nat. Biotechnol*. **36**, 566–569 (2018).
77. Bolger, A. M., Lohse, M. & Usadel, B. Trimmomatic: a flexible trimmer for Illumina sequence data. *Bioinformatics* **30**, 2114–2120 (2014).
78. Bankevich, A. et al. SPAdes: a new genome assembly algorithm and its applications to single-cell sequencing. *J. Comput. Biol*. **19**, 455–477 (2012).
79. Karst, S. M., Kirkegaard, R. H. & Albertsen, M. mmgenome: a toolbox for reproducible genome extraction from metagenomes. Preprint at https://www.biorxiv.org/content/10.1101/059121v1.full (2016).
80. Langmead, B. & Salzberg, S. L. Fast gapped-read alignment with Bowtie 2. *Nat. Methods* **9**, 357–359 (2012).
81. Chen, I. A. et al. IMG/M v.5.0: an integrated data management and comparative analysis system for microbial genomes and microbiomes. *Nucleic Acids Res*. **47**, D666–D677 (2019).
82. NCBI Resource Coordinators. Database resources of the National Center for Biotechnology Information. *Nucleic Acids Res*. **46**, D8–D13 (2018).
83. Bagos, P. G., Liakopoulos, T. D., Spyropoulos, I. C. & Hamodrakas, S. J. PRED-TMBB: a web server for predicting the topology of β-barrel outer membrane proteins. *Nucleic Acids Res*. **32**, W400–W404 (2004).
84. Federhen, S. The NCBI taxonomy database. *Nucleic Acids Res*. **40**, D136–D143 (2012).
85. Parks, D. H., Imelfort, M., Skennerton, C. T., Hugenholtz, P. & Tyson, G. W. CheckM: assessing the quality of microbial genomes recovered from isolates, single cells, and metagenomes. *Genome Res*. **25**, 1043–1055 (2015).
86. Pruesse, E., Peplies, J. & Glöckner, F. O. SINA: accurate high-throughput multiple sequence alignment of ribosomal RNA genes. *Bioinformatics* **28**, 1823–1829 (2012).
87. Ronquist, F. et al. MrBayes 3.2: efficient Bayesian phylogenetic inference and model choice across a large model space. *Syst. Biol*. **61**, 539–542 (2012).
88. Letunic, I. & Bork, P. Interactive tree of life (iTOL) v3: an online tool for the display and annotation of phylogenetic and other trees. *Nucleic Acids Res*. **44**, W242–W245 (2016).
89. Stamatakis, A. RAxML version 8: a tool for phylogenetic analysis and post-analysis of large phylogenies. *Bioinformatics* **30**, 1312–1313 (2014).
90. Sievers, F. et al. Fast, scalable generation of high-quality protein multiple sequence alignments using Clustal Omega. *Mol. Syst. Biol*. **7**, 539 (2011).
91. Lever, M. A. et al. A modular method for the extraction of DNA and RNA, and the separation of DNA pools from diverse environmental sample types. *Front. Microbiol*. **6**, 476 (2015).
92. Kopylova, E., Noé, L. & Touzet, H. SortMeRNA: fast and accurate filtering of ribosomal RNAs in metatranscriptomic data. *Bioinformatics* **28**, 3211–3217 (2012).
93. Bray, N. L., Pimentel, H., Melsted, P. & Pachter, L. Near-optimal probabilistic RNA-seq quantification. *Nat. Biotechnol*. **34**, 525–527 (2016).
94. Pimentel, H., Bray, N. L., Puente, S., Melsted, P. & Pachter, L. Differential analysis of RNA-seq incorporating quantification uncertainty. *Nat. Methods* **14**, 687–690 (2017).
95. van Waasbergen, L. G., Hildebrand, M. & Tebo, B. M. Identification and characterization of a gene cluster involved in manganese oxidation by spores of the marine *Bacillus* sp. strain SG-1. *J. Bacteriol*. **178**, 3517–3530 (1996).
96. Jung, W. K. & Schweisfurth, R. Manganese oxidation by an intracellular protein of a *Pseudomonas* species. *Z. Allg. Mikrobiol*. **19**, 107–115 (1979).
97. Esteve-Núñez, A., Rothermich, M., Sharma, M. & Lovley, D. Growth of *Geobacter sulfurreducens* under nutrient-limiting conditions in continuous culture. *Environ. Microbiol*. **7**, 641–648 (2005).
98. Neubauer, S. C., Emerson, D. & Megonigal, J. P. Life at the energetic edge: kinetics of circumneutral iron oxidation by lithotrophic iron-oxidizing bacteria isolated from the wetland-plant rhizosphere. *Appl. Environ. Microbiol*. **68**, 3988–3995 (2002).
99. Nowka, B., Daims, H. & Spieck, E. Comparison of oxidation kinetics of nitrite-oxidizing bacteria: nitrite availability as a key factor in niche differentiation. *Appl. Environ. Microbiol*. **81**, 745–753 (2015).
100. Ehrich, S., Behrens, D., Lebedeva, E., Ludwig, W. & Bock, E. A new obligately chemolithoautotrophic, nitrite-oxidizing bacterium, *Nitrospira moscoviensis* sp. nov. and its phylogenetic relationship. *Arch. Microbiol*. **164**, 16–23 (1995).
101. Kim, S. & Lee, S. B. Catalytic promiscuity in dihydroxy-acid dehydratase from the thermoacidophilic archaeon *Sulfolobus solfataricus*. *J. Biochem*. **139**, 591–596 (2006).
102. Safarian, S. et al. Structure of a bd oxidase indicates similar mechanisms for membrane-integrated oxygen reductases. *Science* **352**, 583–586 (2016).
103. Lovley, D. R. & Phillips, E. J. P. Manganese inhibition of microbial iron reduction in anaerobic sediments. *Geomicrobiol. J*. **6**, 145–155 (1988).
104. Perez-Benito, J. F., Arias, C. & Amat, E. A kinetic study of the reduction of colloidal manganese dioxide by oxalic acid. *J. Colloid Interface Sci*. **177**, 288–297 (1996).

Acknowledgements This work was supported by NASA Astrobiology Institute Exobiology grant #80NSSC19K0480; and by Caltech's Center for Environmental Microbial Interactions and Division of Geological and Planetary Sciences. We thank S. Connon for assistance with iTag sequencing preparations; G. Rossman and U. Lingappa for spectroscopic analyses and minerology insights; G. Chadwick for discussions on physiology and bioenergetics; I. Antoshechkin and V. Kumar for assistance with nucleic acid library preparation and sequencing at the Millard and Muriel Jacobs Genetics and Genomics Laboratory; N. Dalleska for assistance with ICP–MS analyses at the Environmental Analysis Center; F. Gao for inputs on RNA data analysis using kallisto software at the Bioinformatics Resource Center in the Beckman Institute; C. Ma for assistance with SEM analyses at the GPS Analytical Facility; Y. Guan for assistance with nanoSIMS analyses at the GPS Microanalysis Center; and multiple colleagues for feedback before publication.

Author contributions H.Y. and J.R.L. together applied for funding, designed and conducted the experiments, performed data analyses, prepared the figures and wrote the manuscript.

Competing interests The authors declare no competing interests.

Additional information

Supplementary information is available for this paper at https://doi.org/10.1038/s41586-020-2468-5.

Correspondence and requests for materials should be addressed to J.R.L.

Peer review information *Nature* thanks Edward F. DeLong, Philip Hugenholtz, Bradley M. Tebo, Michael Wagner and the other, anonymous, reviewer(s) for their contribution to the peer review of this work.

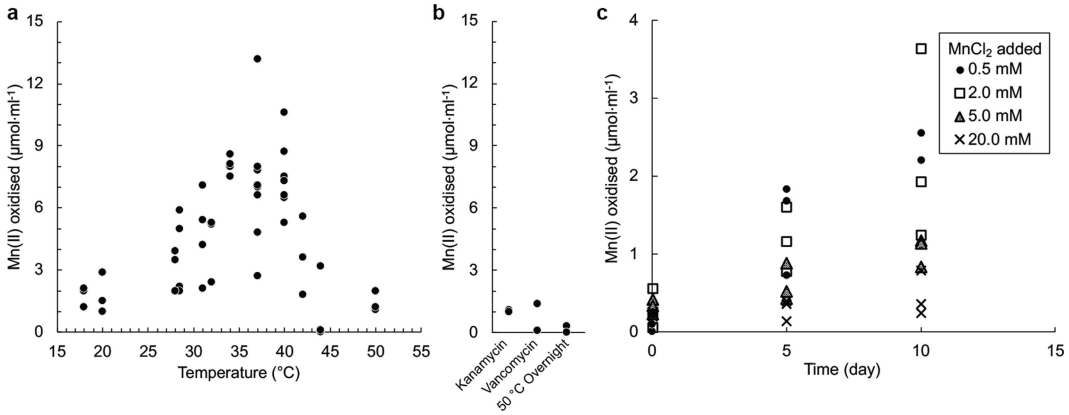

Extended Data Fig. 1 | Effect of temperature, anti-bacterials and Mn(II)Cl_2 on biological Mn(II)CO_3 oxidation. a, Incubation temperature influences oxidation. An optimum between 34 °C and 40 °C was observed, but above these temperatures oxidation was inhibited. By contrast, non-biological reactions would generally be predicted to continue to increase in rate with increasing temperature. **b**, Sensitivity of Mn(II) oxidation to the presence of either of two antibiotics, or to prior pasteurization before extended incubation at 32 °C. **c**, When amended to active co-cultures at concentrations >2.0 mM, $MnCl_2$ appeared to inhibit $MnCO_3$ oxidation when an active culture containing about 2.2 mM unreacted $MnCO_3$ was used as the inoculum. The number of points for each experimental condition represents independent cultivation experiments.

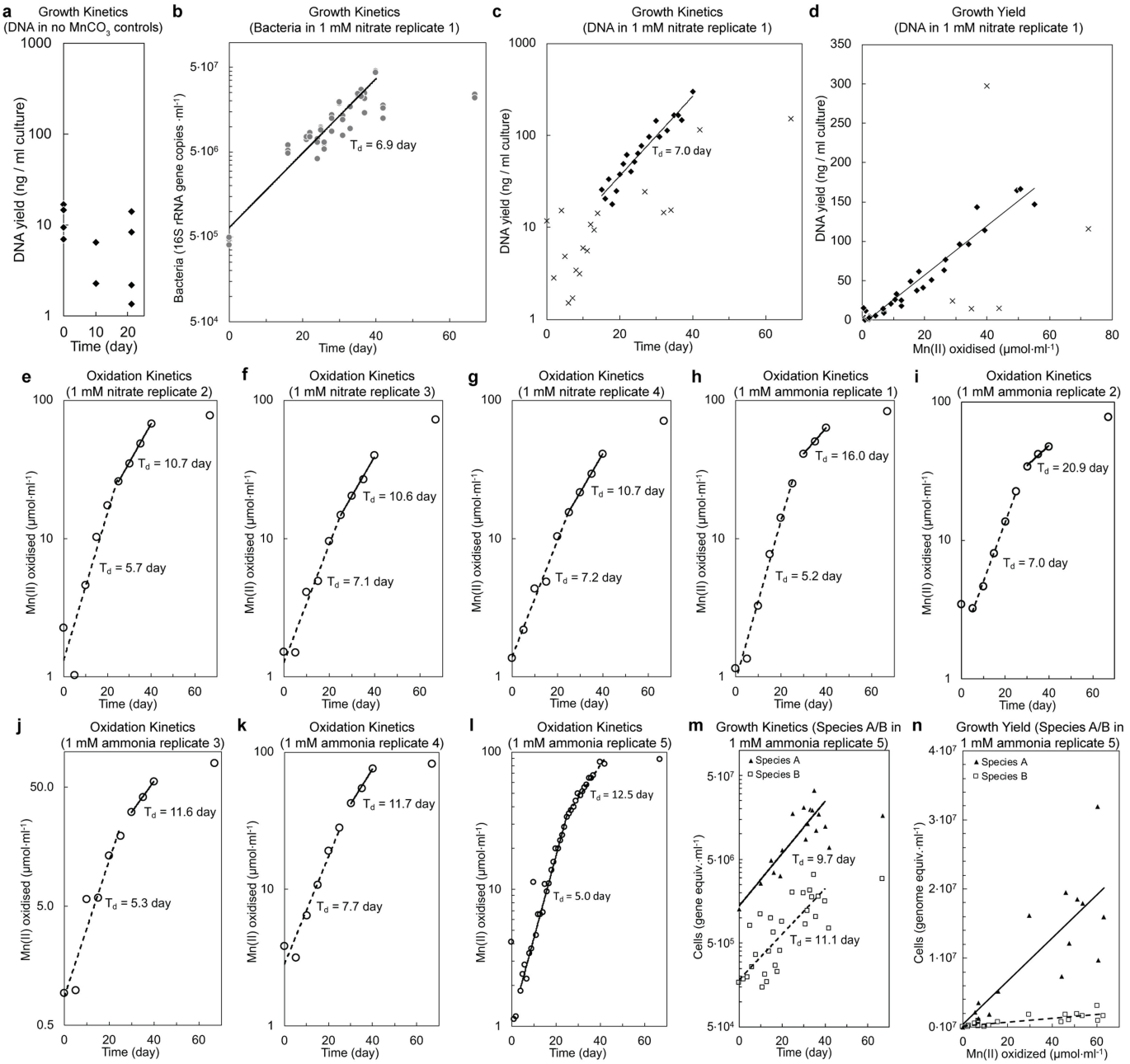

Extended Data Fig. 2 | Mn(II) oxidation and growth by the co-culture. a, DNA yield of the two-species co-culture incubated in MOPS-buffered basal medium in the absence of Mn(II) substrate. No statistically significant changes in the mean DNA yields ($P = 0.06$, day 0 vs 10; $P = 0.70$, day 10 vs 21; $P = 0.20$, day 0 vs 21; two-tailed t-test with equal variance) are observed over the incubation period. **b**, **c**, Exponential increase in bacteria and biomass yields in a Mn(II)-oxidizing culture, which is coupled to exponential increases Mn(II) oxidation (same culture analysed in Fig. 2). Bacteria were measured via 16S rRNA gene copies using a general bacteria probe in quantitative PCR; points represent 3 technical replicates. Biomass was measured via DNA yield from same culture volumes. **d**, Exponential increases in Mn(II) oxidation (Fig. 2a) and DNA yields by this same culture (1 mM nitrate replicate 1, **c**) correlate. Similar relationships were observed in samples from independent cultivation experiments ($n = 2$). **e**–**l**, Kinetics of Mn(II) oxidation by the co-culture in basal medium; two phases of exponential Mn(II) oxidation were observed. **e**–**g**, Basal medium with 1 mM nitrate ($n = 4$; for replicate 1, see **b**–**d** and Fig. 2). **h**–**l**, Basal medium with 1 mM ammonia ($n = 5$). **m**, Exponential growth of species A and species B paralleled Mn(II) oxidation in basal medium with 1 mM ammonia as the nitrogen source (1 mM ammonia replicate 5, **l**), rather than 1 mM nitrate. **n**, Linear relationship between cell growth and the amount of Mn(II) oxidized (1 mM ammonia replicate 5, **l** and **m**). Values in **n** were normalized by subtracting the initial cell number and Mn oxide concentrations at the onset of the experiment, and negative values after normalization were excluded from the analysis. All data points included in the line fits are used to calculate the doubling times (T_d), unless otherwise noted by 'x' symbols.

a

	FISH Microscopy (cells)*	16S rRNA iTag Sequencing (PCR amplified sequences)†	Metagenome (binned reads)‡	Metatranscriptome (assigned reads)§
Species A	5.1 (s.d. = 1.5, n=3)	6.5 (s.d. = 1.2, n=6)	16.5 (n=1)	36 (s.d. = 18, n=7)
Species B	1	1	1	1

b Mn(II) oxidation by Species A

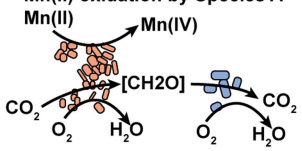

c Micro-nutrient based consortia

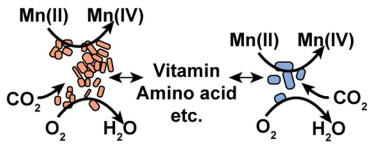

d Electron acceptor based consortia

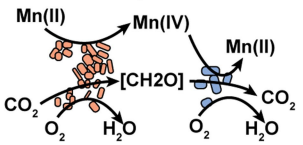

e Electron donor based consortia

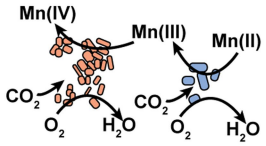

f

	Ca. Manganitrophus noduliformans (Species A)	*Ramlibacter lithotrophicus* (Species B)
Genome size (bp)	5171380	5263905
Number of scaffolds	22	24
GC content	56.41%	69.03%
Total gene count	4890	5082
Genome completeness estimate[85]	97.41%	98.28%
Genome contamination estimate[85]	0.00%	0.00%
Proportion of sequence reads in the co-culture	91.83%	5.71%
SSU rRNA count	1	2
GOLD Analysis Project Id	Ga0306812	Ga0265800
IMG Genome ID	2784132095	2778260901
GenBank accession number	VTOW00000000	VTOX00000000

g

Organism	Metabolism	Substrate consumption rate (mol substrate·cell^{-1}·hr^{-1})	Cell yield (cell·mol^{-1} substrate)	Protein yield (mg·mol^{-1} substrate)	Doubling time (hr)	References
Species A + Species B Co-culture	Mn(II) ox	$9.0 \cdot 10^{-15}$	$7.4 \cdot 10^{11}$	115‖	156	This study¶ (with nitrate)
Bacillus sp. SG-1	Mn(II) ox	$2 \cdot 10^{-15}$	(not Mn driven)	-	-	95
Pseudomonas putida MnB1	Mn(II) ox	$2.8 \cdot 10^{-16}$ to $6.6 \cdot 10^{-16}$	(not Mn driven)	-	-	96
Shewanella oneidensis MR-1	Mn(IV) red	$0.2 \cdot 10^{-15}$ to $8.7 \cdot 10^{-15}$	$3.2 \cdot 10^{13}$ to $16.1 \cdot 10^{13}$	4928 to 24794‖	na	5
Geobacter sulfurreducens	Fe(III) red	$5.3 \cdot 10^{-15}$	na	na	na	97
Sideroxydans paludicola BrT	Fe(II) ox	$4.2 \cdot 10^{-14}$	$5.8 \cdot 10^{13}$ ‖	385‖	25	98
S. lithotrophicus ES-1	Fe(II) ox	na	na	na	8	26
S. lithotrophicus ES-2	Fe(II) ox	na	na	na	12.5	26
Ca. Nitrospira defluvii	NO_2^- ox	$2.8 \cdot 10^{-15}$	$8.5 \cdot 10^{12}$	122	37	99
Nitrospira moscoviensis	NO_2^- ox	$0.6 \cdot 10^{-15}$	$7.7 \cdot 10^{11}$ to $3.5 \cdot 10^{13}$	120 to 509	12 to 119	39,99,100
Nitrospira strain BS10	NO_2^- ox	$2.1 \cdot 10^{-15}$	$2.5 \cdot 10^{13}$	142	37	99
Nitrospira inopinata	NH_3 ox	$2.3 \cdot 10^{-15}$ ‖	$2.5 \cdot 10^{12}$ ‖	395	na	23

na, not available.

h

Sample	% Mn(II) oxidised	Total reads	Trimmed reads	rRNA reads	% rRNA mapped to Species A	% rRNA mapped to Species B	non_rRNA reads	% non_rRNA	% non_rRNA mapped to co-culture	% non_rRNA mapped to Species A	% non_rRNA mapped to Species B
Mn03	77%	109091889	106711024	77092676	97.9566%	1.7069%	29618348	27.76%	92.80%	92.93%	7.32%
Mn06	73%	100999745	98689865	71725792	92.2632%	6.8944%	26964073	27.32%	93.32%	94.86%	5.36%
Mn08	66%	110162236	107964879	88883019	98.0882%	1.6077%	19081860	17.67%	94.86%	97.55%	2.59%
Mn09	19%	115815146	113931273	93687311	97.4873%	2.4631%	20243962	17.77%	98.01%	98.12%	2.00%
Mn10	45%	116250176	114219564	91931244	98.1423%	1.8191%	22288320	19.51%	98.03%	98.73%	1.42%
Mn11	61%	113561784	111575708	86707597	97.4281%	2.5316%	24868111	22.29%	98.20%	97.67%	2.49%
Mn12	18%	11905263	11905263	10978600	95.5201%	3.1230%	755906	6.4%	89.13%	96.49%	3.66%

Extended Data Fig. 3 | See next page for caption.

Extended Data Fig. 3 | Properties of the refined co-culture. a, Estimations of the relative ratio between species A and species B. ∗Slow-growing microorganisms, in particular species A (which also has a smaller cell volume than species B or *Escherichia coli*) could have a lower number of ribosomes, resulting in lower signal intensity from rRNA-targeted fluorescent probes, relative to the fluorescent signal from DNA stain DAPI. †The two species together account for 99.7% of assigned sequence reads (Supplementary Table 1). ‡The two species together account for 97.54% of the sequence reads in the metagenome (**f**). §The two species together account for 99.576% (s.d. = 0.005%, $n = 7$) of the rRNA sequence reads and 100.1700% (s.d. = 0.0005%, $n = 7$) of the non-rRNA sequence reads in the co-culture metatranscriptomes (**h**). **b**–**e**, Possible metabolic interactions that may be occurring between species A (orange) and species B (blue). **f**, Genome statistics for species A and species B. **g**, Observed rates and yields of Mn(II) oxidation by the co-culture, in comparison to the literature values[5,23,26,39,95–100] reported for other physiologically or phylogenetically related lithotrophs or metal-active heterotrophs. ‖Conversion estimate based on *Escherichia coli* biomass of 2.8×10^{-13} g dry cell weight per cell, of which 55% is protein[27]. ¶Co-culture values correspond to results from the single independent culture with nitrate as the nitrogen source for which extensive data on both oxidation kinetics and growth (genome copies) were collected. **h**, Transcriptome statistics for 7 co-cultures sampled at different degrees of Mn(II) oxidation.

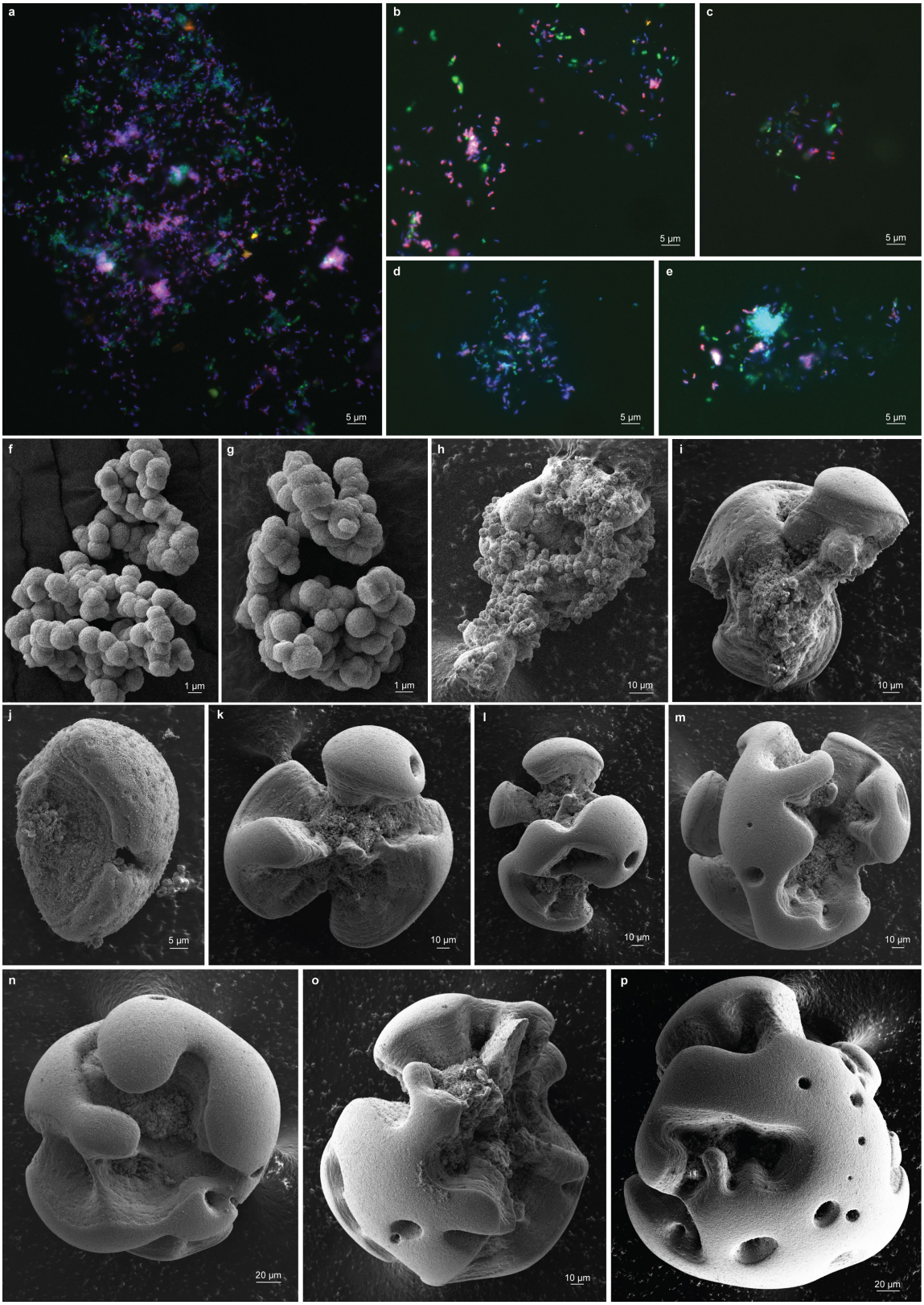

Extended Data Fig. 4 | Microscopy of Mn oxide nodules formed by the co-culture. a–**e**, Epifluorescence microscopy reveals distribution of cells of species A and species B associated with dissolved Mn oxide nodules. DAPI (blue) was used to stain DNA, in addition to applying species-specific FISH probes targeting the 16S rRNA of species A (magenta) and species B (green). Probe fluorescence for species A was dim and faded rapidly, but was associated with the cells that otherwise appear in photomicrographs to only be DAPI-stained. No third species is present, as observed in independent cultivation experiments ($n = 2$), and confirmed via independent methods (Extended Data Fig. 3a). **f**–**p**, Scanning electron micrographs of Mn(II)CO_3 substrate (**f**, **g**) and Mn oxide nodules collected from liquid cultures (**h**–**p**). Representative nodules are from independent cultivation experiments ($n = 4$).

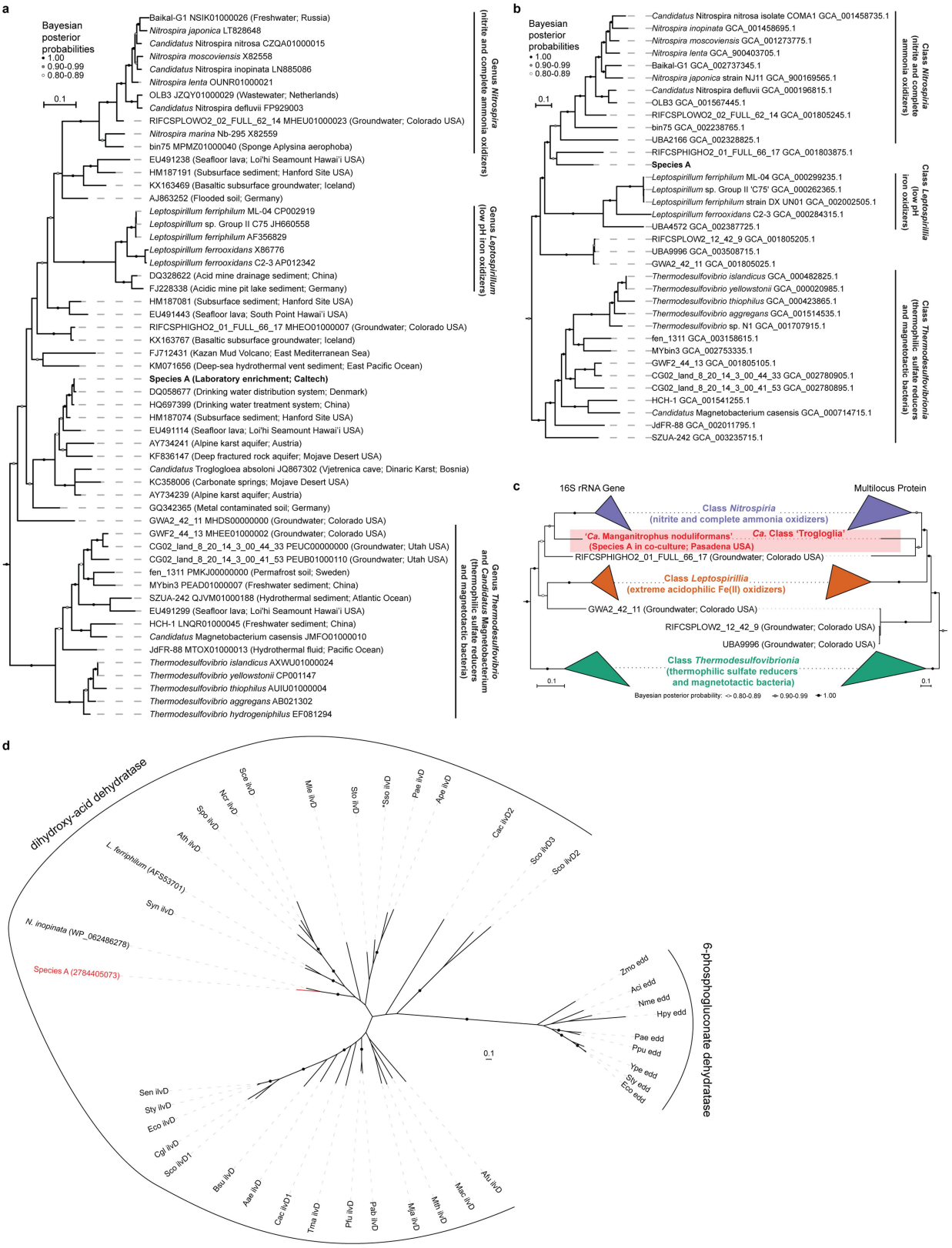

Extended Data Fig. 5 | See next page for caption.

Extended Data Fig. 5 | Phylogenetic analyses on species A. a, 16S rRNA gene phylogram, based on a Bayesian analysis of 1,532 aligned nucleotide positions. NCBI[82] taxonomic classifications are used, and sequences shown are all from the phylum Nitrospirae. The names and known physiologies for the previously described genera in this phylum are shown on the right. NCBI accession numbers for 16S rRNA sequences are included in the node names. Source environment for the sequences are shown in brackets. **b**, Multilocus phylogram, based on a Bayesian analysis of 5,036 aligned amino acid positions concatenated from 120 bacterial protein markers[62]. GTDB[62] taxonomic classifications are used, and sequences shown are from the phylum under the headings 'Nitrospirota' and 'Nitrospirota_A'. The names and known physiologies for the previously described classes in this phylum are shown on the right. NCBI accession numbers for genome assemblies are included in the node names. For **a**, **b**, the dots on the branches indicate posterior probabilities greater than 0.80. **c**, Phylogenetic analyses of the phylum Nitrospirae (Nitrospirota) limited to only those species with reconstructed genomes yield a topology different from that observed in **a** and Fig. 3a. Bayesian phylogram based on 1,532 aligned 16S rRNA nucleotide positions (left); multilocus Bayesian phylogram, based on 5,036 aligned amino acid positions of 120 concatenated bacterial protein markers (right). Sequences clustering within the three previously described classes within this phylum are collapsed into separate nodes. **d**, Protein sequence phylogeny of dihydroxy-acid and 6-phosphogluconate dehydratases. Sequences were selected based on a previous study[101], with the addition of homologues found in *Nitrospira inopinata*, *Leptospirillum ferriphilum* and species A (red). All 770 aligned amino acid positions were used in the maximum likelihood analysis. Protein accession numbers from the NCBI database or gene identifiers from the IMG database of the 3 new sequences are shown in parentheses. Black dots on the branches represent bootstrap values equal to 100%. Although dihydroxy-acid dehydratase and 6-phosphogluconate dehydratase are homologous, they form separate clusters phylogenetically as reported[101]. The homologues in Nitrospirae all belong to the dihydroxy-acid dehydratase clade, therefore are unlikely candidates for 6-phosphogluconate dehydratase activity and function in the ED pathway. All scale bars show evolutionary distance (0.1 substitutions-per-site average).

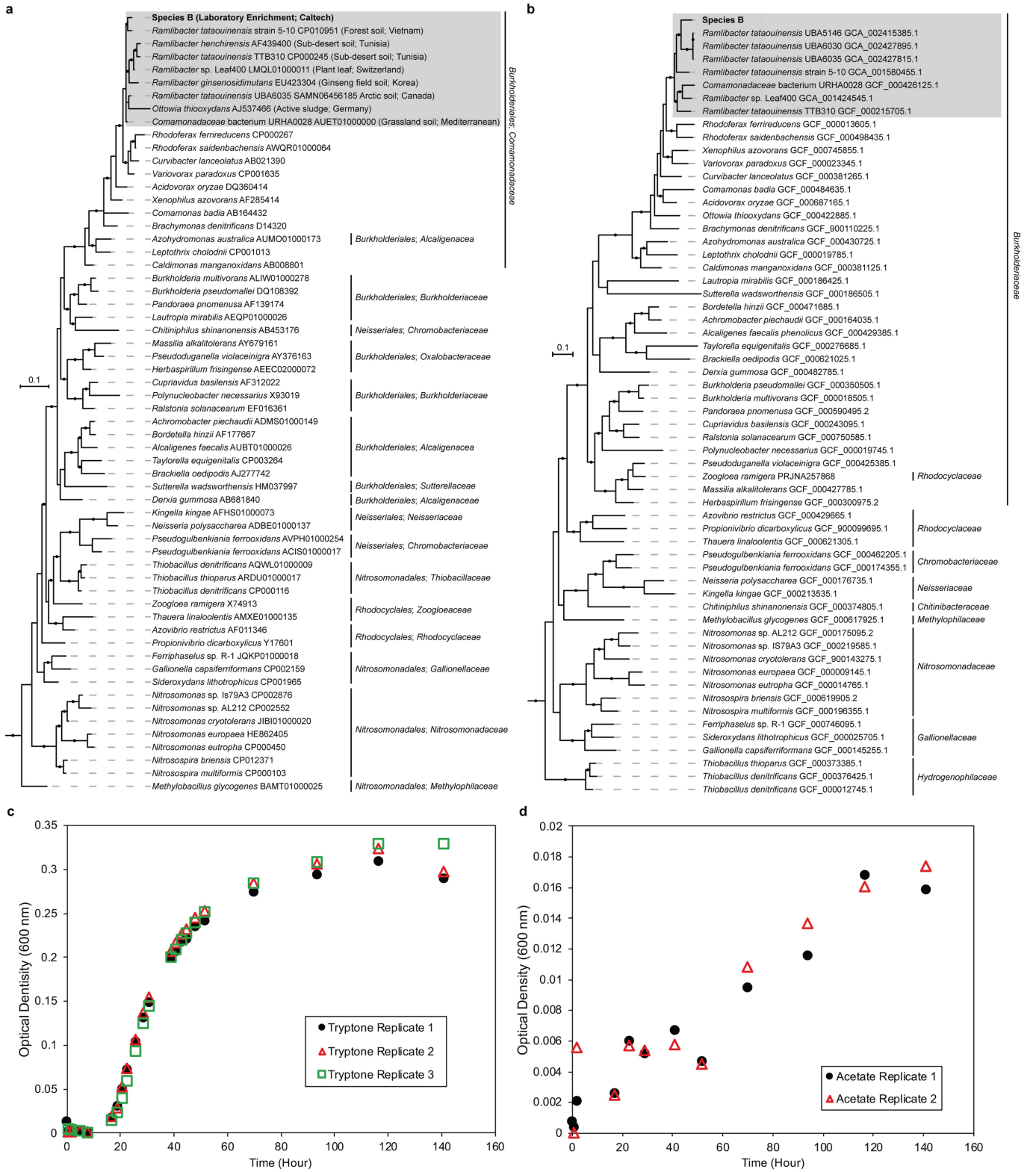

Extended Data Fig. 6 | Phylogenetic analyses and aerobic heterotrophic growth of isolated species B. a, 16S rRNA gene phylogram, based on a Bayesian analysis of 1,532 aligned nucleotide positions. NCBI[82] taxonomic classifications are used, with sequences selected from the class Betaproteobacteria. The genus *Ramlibacter*, consistently identified in two phylogenetic approaches, is shaded in grey, with species B in bold. Source environments for the species in *Ramlibacter* are shown in brackets. The order and family classifications are included to the right separated by a semicolon. The black dots on the branches indicate posterior probabilities greater than 0.90. **b**, Multilocus phylogram, based on a maximum-likelihood analysis of 5,035 aligned amino acid positions concatenated from 120 bacterial protein markers[62]. GTDB[62] taxonomic classifications are used, and sequences shown are from the order Betaproteobacteriales. The GTDB family classifications are included to the right of species names. NCBI accession numbers for 16S rRNA sequences or the genome assemblies are included after the species names. The black dots on the branches indicate bootstrap values greater than 90%. Scale bars shown evolutionary distance (0.1 substitutions-per-site average). **c**, **d**, Kinetics of species B growth basal media with either 5 g/l of tryptone ($n = 3$ biological replicates) (**c**) or 10 mM acetate ($n = 2$ biological replicates) (**d**).

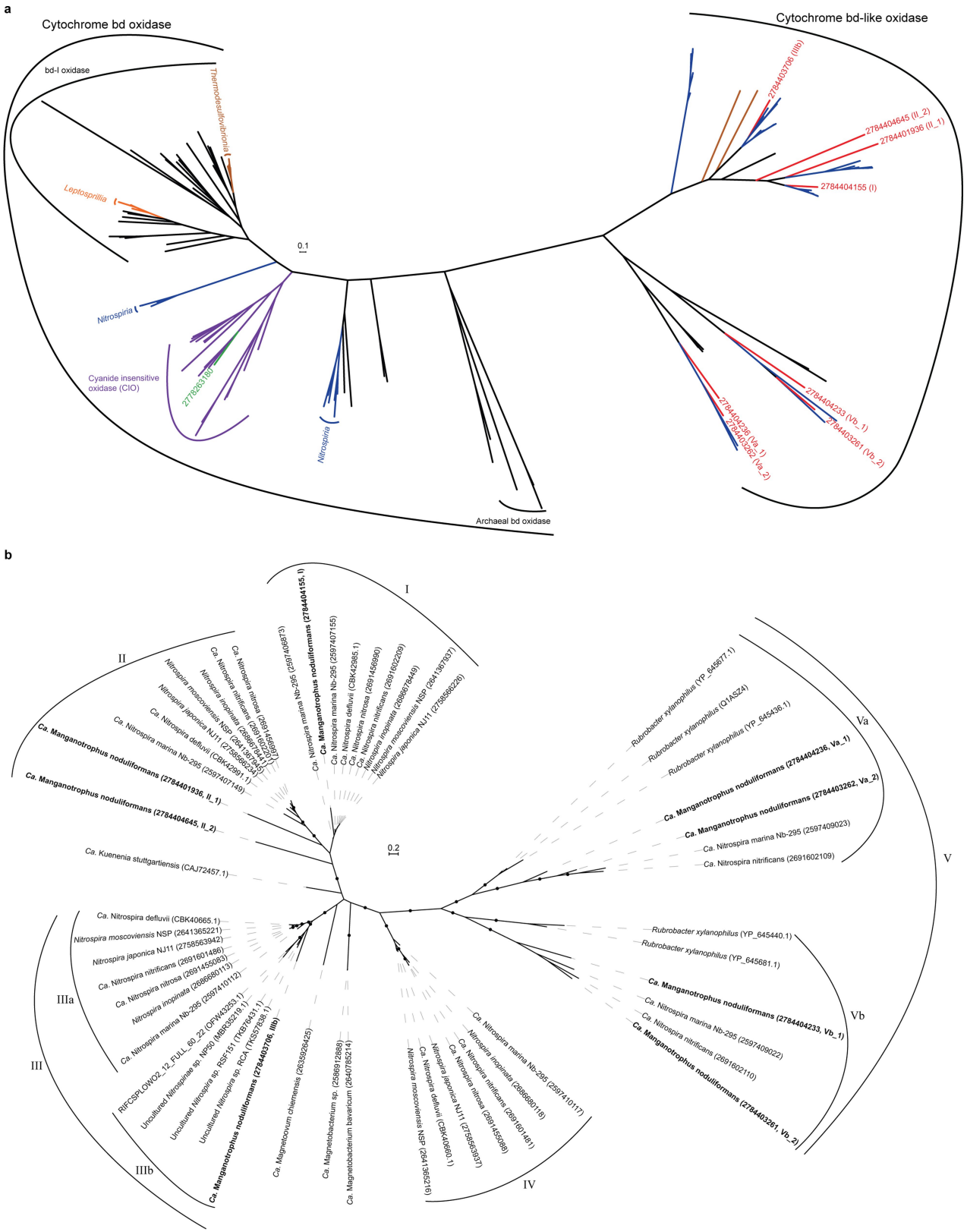

Extended Data Fig. 7 | See next page for caption.

Extended Data Fig. 7 | Phylogenetic analyses of cytochrome *bd* oxidase subunit I and cytochrome *bd*-like oxidases. Only cytochrome *bd*-like oxidases were identified in species A, in contrast to other classes in the phylum Nitrospirae (Nitrospirota). **a**, Unrooted maximum-likelihood tree, constructed using 242 amino acid positions shared between cytochrome *bd* and *bd*-like oxidases, using RAxML[89] (model LGF). Deduced proteins from the genome of species A are in red, with their IMG gene identifiers and clade numbering (as shown in Fig. 3b) included in brackets. Other proteins from the phylum Nitrospirae (Nitrospirota) are coloured blue, orange or brown for classes Nitrospiria, Leptospirillia or Thermodesulfovibrionia, respectively. Cytochrome *bd* oxidase of species B, with its IMG identifier, is in green; it belongs to the cyanide insensitive oxidase clade in purple. **b**, Phylogenetic analysis of cytochrome *bd*-like oxidases from species A. Unrooted maximum-likelihood tree was constructed using 242 amino acid positions shared between different clades of cytochrome *bd*-like oxidases. Cytochrome *bd*-like oxidases are assigned to different clades, based on the phylogeny and their gene cluster structures. Species A encodes 8 cytochrome *bd*-like oxidases (bold), representing clades I, II, IIIb, Va and Vb; clade numbering as shown in Fig. 3b are included in brackets after the IMG identifiers. Black dots on branches represent bootstrap values greater than 90%. Scale bars show evolutionary distance (substitutions-per-site average).

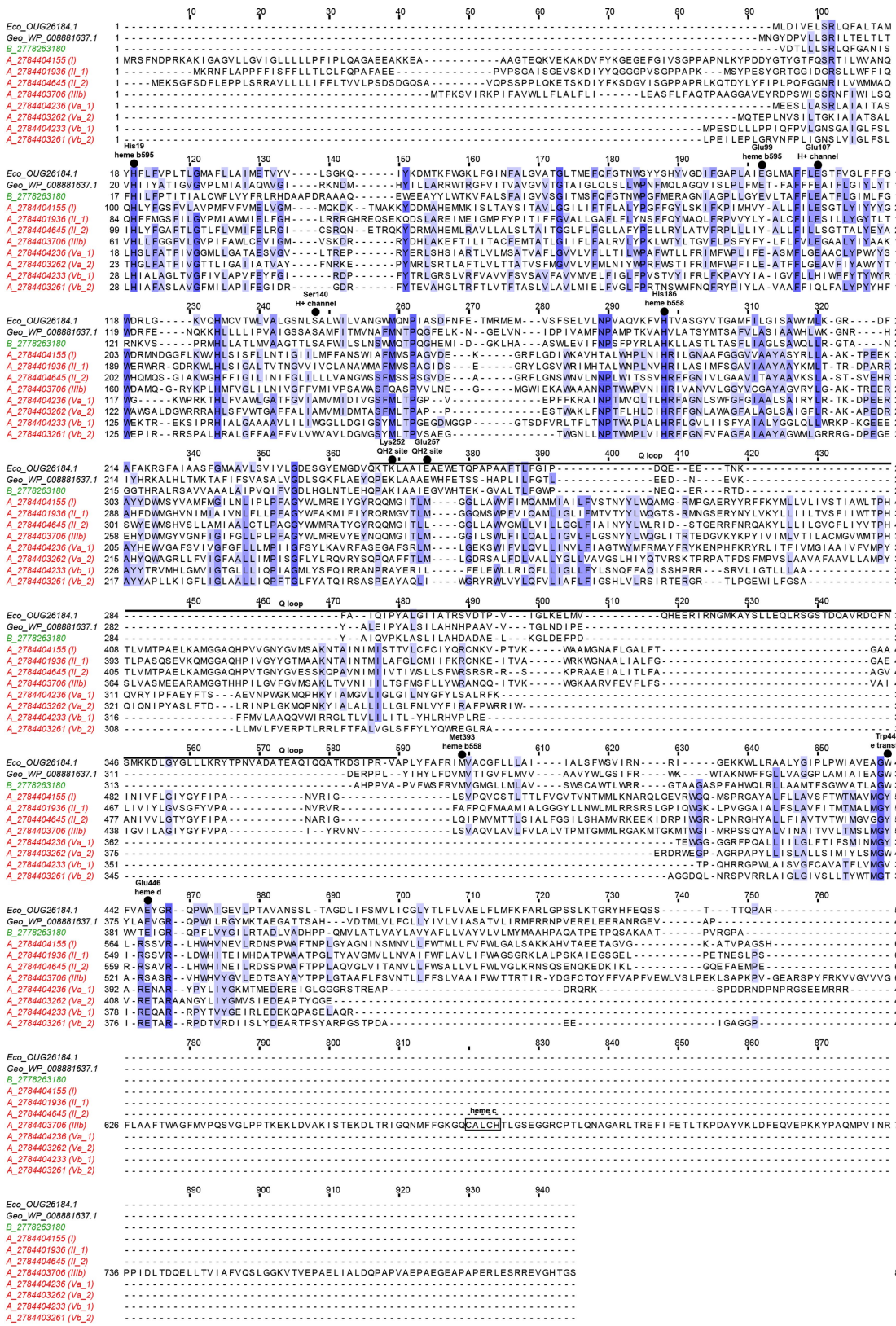

Extended Data Fig. 8 | Sequence alignment of cytochrome *bd* and *bd*-like oxidases. Cytochrome *bd*-like oxidase in species A (sequence names starting with A, followed by their IMG gene identifier and clade numbering as shown in brackets in Fig. 3b) and cytochrome *bd* oxidase subunit I in species B (sequence name starting with B, followed by its IMG gene identifier) are aligned to characterized cytochrome *bd* oxidases in *Escherichia coli* (sequence name starting with Eco, followed by its NCBI identifier) and *Geobacillus thermodenitrificans* (sequence name starting with Geo, followed by its NCBI identifier). Key features as revealed by structure[102] are indicated at the top of the alignment, using *E. coli* protein residue numbering. The cytochrome *bd* oxidase subunit I sequence from species B shows conservation of all key residues. By contrast, cytochrome *bd*-like oxidases in species A do not show conservation of many key residues; instead, they are predicted to have up to 14 transmembrane helices (compared to 9 in *E. coli*). One cytochrome *bd*-like oxidase in species A has a C-terminus extension with a haem *c* binding motif (CXXCH).

a

Stable Isotope Probing	Species	FISH-nanoSIMS		nanoSIMS without paraformaldehyde fixation or FISH	
		^{13}C atom percent	^{15}N atom percent	^{13}C atom percent	^{15}N atom percent
$MnCO_3$ + $Na^{15}NO_3$	A	1.06 (s.d=0.02, n=33)	64.25 (s.d=9.76, n=33)	1.07 (s.d=0.02, n=54)	71.03 (s.d=2.60, n=54)
	B	1.04 (s.d=0.03, n=7)	23.74 (s.d=15.65, n=7)	1.10 (s.d=0.06, n=20)	9.87 (s.d=10.06, n=20)
$Mn^{13}CO_3$ + $Na^{15}NO_3$	A	35.57 (s.d=9.57, n=107)	57.59 (s.d=8.20, n=107)	56.56 (s.d=6.51, n=394)	69.01 (s.d=6.34, n=394)
	B	7.93 (s.d=5.62, n=27)	15.77 (s.d=13.30, n=27)	10.52 (s.d=8.20, n=130)	11.71 (s.d=9.31, n=130)

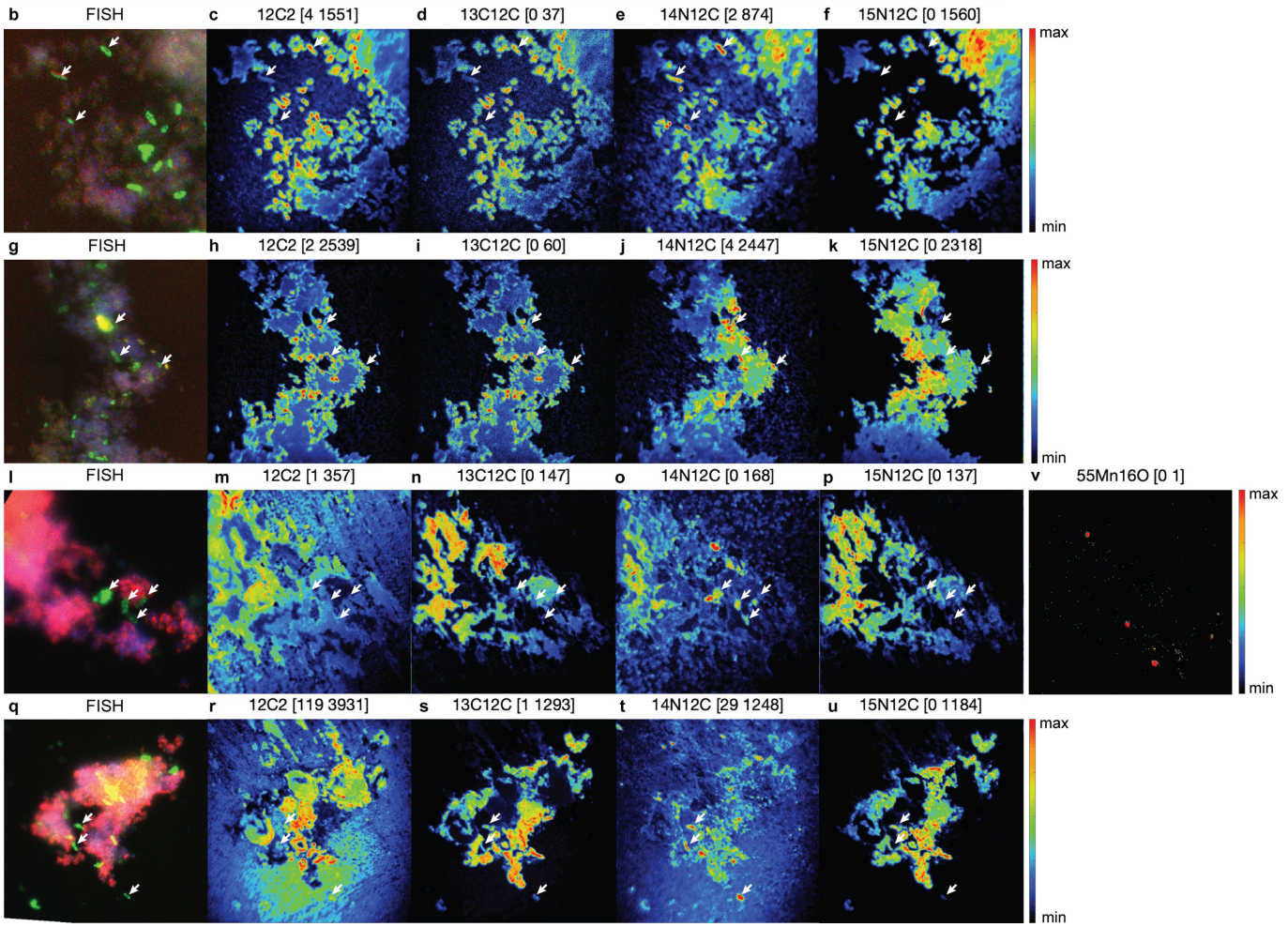

Extended Data Fig. 9 | Stable isotope probing of Mn(II)-oxidizing co-culture measured using nanoSIMS. a, Summary of stable isotope probing analysis of cells dissolved from Mn oxide nodules, either with paraformaldehyde fixation and FISH, or without (to avoid dilution with natural abundance isotopes). Cells of species A and species B were either identified by FISH or by elemental composition (species B cells were observed to have higher $^{14}N/^{15}N$ ratios), and their isotopic compositions were obtained via nanoSIMS (n = the total number of cell regions of interest analysed in the nanoSIMS images). For FISH–nanoSIMS analyses, a total of 2 and 5 nanoSIMS images from single cultures incubated with either $MnCO_3$ or $Mn^{13}CO_3$, respectively, was examined. For nanoSIMS analyses without paraformaldehyde fixation and FISH, a total of 3 and 17 nanoSIMS images from single cultures incubated with either $MnCO_3$ or $Mn^{13}CO_3$, respectively, was examined. **b**–**u**, Individual secondary ion images from nanoSIMS showing incorporation of inorganic ^{13}C and ^{15}N into the cells of both species (dissolved from Mn oxide nodules grown in the presence of $MnCO_3$ and $^{15}NO_3^-$ (**b**–**k**) or $Mn^{13}CO_3$ and $^{15}NO_3^-$ (**l**–**u**)), and species B cells could have higher ^{14}N content than species A. Secondary ions $^{12}C_2^-$ (mass 24 for ^{12}C), $^{13}C^{12}C^-$ (mass 25 for ^{13}C), $^{14}N^{12}C^-$ (mass 26 for ^{14}N), $^{15}N^{12}C^-$ (mass 27 for ^{15}N), $^{32}S^-$ (mass 32 for ^{32}S) were simultaneously measured. The counts of the secondary ions are shown in brackets (minimum–maximum) and displayed using the colour scale shown to the right of the images. **b**–**f** and **l**–**p** correspond to the top and bottom panels in Fig. 4, respectively. White arrows indicate species B cells identified in FISH showing high ^{14}N in nanoSIMS. **v**, NanoSIMS measurement of residual Mn associated with cells grown with $Mn^{13}CO_3$ and $^{15}NO_3^-$, after dissolving from Mn oxide nodules. The same nanoSIMS image area was analysed as in **l**–**p**, except $^{55}Mn^{16}O^-$ (mass 71 for ^{55}Mn) was measured (n = 1 nanoSIMS image) in addition to other secondary ions. Negligible amount of Mn was found in the biomass, indicating that any remaining $Mn^{13}CO_3$ substrate had been completely dissolved away during sample preparation, and thus did not interfere with the ^{13}C analyses.

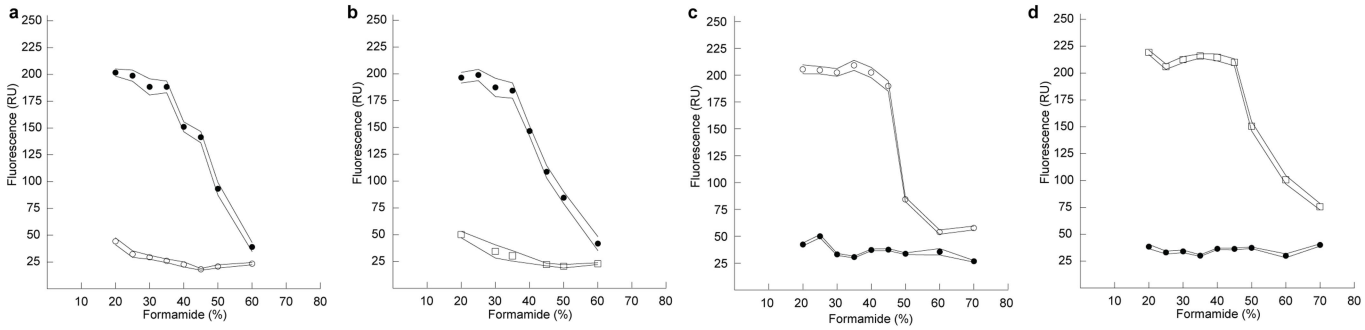

e

Compound	Average Mn Oxidation State	Manufacturer	Mn(II) oxidised or "acid-insoluble fraction" (μmol·ml^{-1})	Mn(II) or "acid-soluble fraction" (μmol·ml^{-1})	Total Mn (μmol·ml^{-1})	Mn(II) oxidised or "acid-insoluble fraction" (%)	Mn(II) or "acid-soluble fraction" (%)
$MnCl_2$	2	Fluka #221279	0.6	86.7	87.3	0.7%	99.3%
$MnSO_4$	2	MPBio #10034-96-5	0.4	88.9	89.3	0.5%	99.5%
MnO	2	Aldrich #377201	0.9	71.1	72.0	1.3%	98.7%
$MnCO_3$-anhydrous	2	Aldrich #377449	1.5	84.6	86.1	1.7%	98.3%
$MnCO_3$·xH_2O	2	Aldrich #53539	1.4	77.2	78.6	1.8%	98.2%
Mn_3O_4	2.7	Aldrich #277473	18.9	85.9	104.8	18.0%	82.0%
Mn_2O_3	3	Aldrich #377457	87.1	75.6	162.7	53.5%	46.5%
MnO_2	4	Synthetized according to 103	170.1	2.0	172.0	98.9%	1.1%
MnO_2	4	Synthetized according to 104	31.0	0.6	31.6	98.2%	1.8%
MnO_2	4	Sigma #310700	72.9	1.2	74.1	98.4%	1.6%
$KMnO_4$	7	Baker #3227-01	16.0	7.7	23.7	67.6%	32.4%

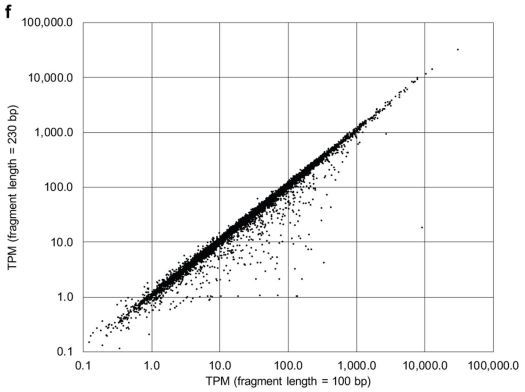

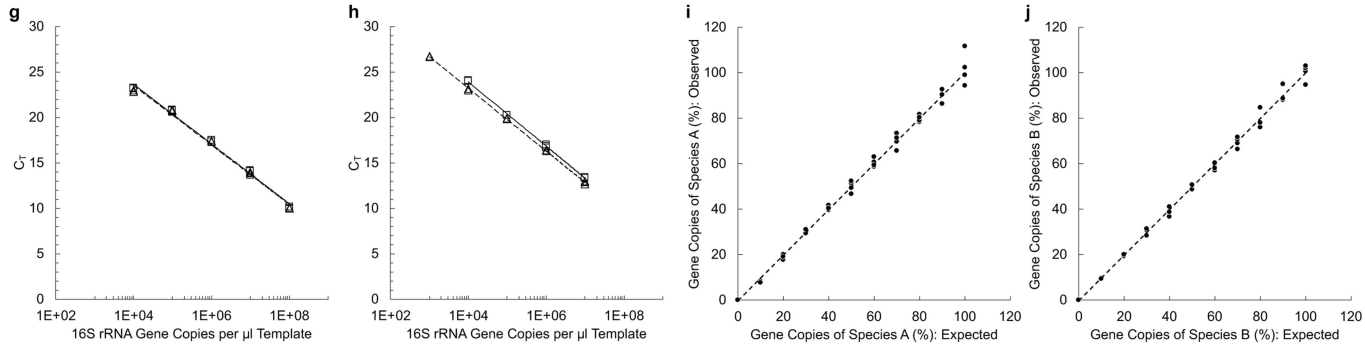

Extended Data Fig. 10 | Evaluations of experimental methods. a–**d**, Evaluation of FISH oligonucleotide probes. Three probes (NLT499, black circles; BET359, white circles; BET867, white squares) were tested in different probe combinations and formamide concentrations, using 16S rRNA gene clones of species A (**a**, **b**) or species B (**c**, **d**). Each point in the dissociation profile represents the mean of fluorescence intensities of at least 100 different single cells in 5 distinct microscopic fields of 1 biological replicate. Lines connect the 95% confidence intervals of the points. No interference was found when targeting either species A or species B with different probe combinations and formamide concentrations. RU, relative units of fluorescence intensity. **e**, Evaluation of ICP–MS method to measure Mn compounds with different oxidation states. Mn(II) in its various forms can be almost entirely measured in the acid-soluble fraction with little in the acid-insoluble fraction, and any increase in the acid-insoluble fraction is an indication of oxidized Mn(II). We refer to the 'acid-soluble fraction' as Mn(II), and the 'acid-insoluble fraction' as Mn(II) oxidized representing Mn(III/IV). Supplementary Note 4 provides more details. MnO_2 was synthesized according to two previously published methods[103,104]. **f**, Evaluation of transcriptome analysis software kallisto[93]. Average fragment length for RNA libraries was measured to be 230 bp. However, using 230 bp as the input parameter for fragment length caused a kallisto[93] expression evaluation issue for genes <230 bp in length; thus, the fragment length was adjusted downward to 100 bp to evaluate the expression of genes <230 bp. This parameter change does not affect the overall transcript expression for genes >230 bp as seen in the correlation analysis, performed using transcriptome sample Mn03. **g**, **h**, Evaluation of quantification range and efficiency of quantitative PCR oligonucleotide probes. Three quantitative PCR oligonucleotide probes (bacteria (**g**) or species A- or species B-specific (**h**)) were tested using cloned 16S rRNA gene of either species A (open squares, solid lines) or species B (open triangles, dashed lines) as DNA templates. Threshold cycle (C_T) versus gene copies show that all three probes had amplification efficiencies between 90–105% in the quantification ranges plotted. Points represent 3 technical replicates. **i**, **j**, Evaluation of specificity of quantitative PCR oligonucleotide probes. The percentage of species A (**i**) and species B (**j**) was estimated in reactions containing a mixture of cloned 16S rRNA genes from both species A and species B as DNA templates. Dashed lines represent theoretical 100% match in the expected versus measured values. The results indicate that the species-specific probes quantified their targeted species with minimal interference. Points represent 4 technical replicates.

nature research

Corresponding author(s): Jared R. Leadbetter

Last updated by author(s): Apr 13, 2020

Reporting Summary

Nature Research wishes to improve the reproducibility of the work that we publish. This form provides structure for consistency and transparency in reporting. For further information on Nature Research policies, see Authors & Referees and the Editorial Policy Checklist.

Statistics

For all statistical analyses, confirm that the following items are present in the figure legend, table legend, main text, or Methods section.

n/a	Confirmed	
☐	☒	The exact sample size (*n*) for each experimental group/condition, given as a discrete number and unit of measurement
☐	☒	A statement on whether measurements were taken from distinct samples or whether the same sample was measured repeatedly
☐	☒	The statistical test(s) used AND whether they are one- or two-sided *Only common tests should be described solely by name; describe more complex techniques in the Methods section.*
☒	☐	A description of all covariates tested
☒	☐	A description of any assumptions or corrections, such as tests of normality and adjustment for multiple comparisons
☐	☒	A full description of the statistical parameters including central tendency (e.g. means) or other basic estimates (e.g. regression coefficient) AND variation (e.g. standard deviation) or associated estimates of uncertainty (e.g. confidence intervals)
☒	☐	For null hypothesis testing, the test statistic (e.g. *F*, *t*, *r*) with confidence intervals, effect sizes, degrees of freedom and *P* value noted *Give P values as exact values whenever suitable.*
☒	☐	For Bayesian analysis, information on the choice of priors and Markov chain Monte Carlo settings
☒	☐	For hierarchical and complex designs, identification of the appropriate level for tests and full reporting of outcomes
☒	☐	Estimates of effect sizes (e.g. Cohen's *d*, Pearson's *r*), indicating how they were calculated

Our web collection on statistics for biologists contains articles on many of the points above.

Software and code

Policy information about availability of computer code

Data collection	Zeiss Stemmi 2000-C stereomicroscope, Zeiss Axioplan 2 Imaging Microscope, Panasonic Lumix GH3 and G85 microfourthirds-lens-mount cameras, Olympus BX51 epifluorescence microscope, Nicolet Magna 860 Fourier transform infrared (FTIR) spectrophotometer, Zeiss 1550VP field emission SEM, Agilent 8800 inductively coupled plasma mass spectrometer, Bio-Rad C1000 Thermal Cycler with CFX96 Real-Time System, Illumina HiSeq2500, Agilent Technologies Bioanalyzer, CAMECA NanoSIMS 50L
Data analysis	Databases: NCBI (ncbi.nlm.nih.gov), JGI IMG (https://img.jgi.doe.gov/cgi-bin/mer/main.cgi), SILVA Ref NR 99 Database Release 119, Genome Taxonomy Database (GTDB) v0.2.2 Data Analysis: QIIME v1.8.0, UCLUST v7.11.0.667, ARB software v6.0.2, SINA v1.2.11, daime v2.1, RTA v1.18.64, bcl2fastq v1.8.4, Trimmomatic v0.36, Spades v3.11.1, mmgenome v0.7.1, bowtie2 v2.3.4.1, CheckM v1.0.6, GTDB v0.2.2, MrBayes v3.2.6, RAxML v8.1.7, sortmerna v2.0, kallisto v0.44.0, sleuth v0.30.0, BBMap v37.93, PRED-TMBB (http://bioinformatics.biol.uoa.gr/PRED-TMBB/), Look@NanoSIMS v2019-05-14 Data Visualization: iTOL (https://itol.embl.de/), Adobe Photoshop CC 2019, Adobe Illustrator CC 2019, Adobe Lightroom CC 2019

For manuscripts utilizing custom algorithms or software that are central to the research but not yet described in published literature, software must be made available to editors/reviewers. We strongly encourage code deposition in a community repository (e.g. GitHub). See the Nature Research guidelines for submitting code & software for further information.

Data

Policy information about availability of data

All manuscripts must include a data availability statement. This statement should provide the following information, where applicable:

- Accession codes, unique identifiers, or web links for publicly available datasets
- A list of figures that have associated raw data
- A description of any restrictions on data availability

All sequencing data has been deposited at National Center for Biotechnology Information (NCBI) under BioProject PRJNA562312. The cloned 16S rRNA gene sequences of “Ca. Manganitrophus noduliformans” (Species A) and Ramlibacter lithotrophicus (Species B) from the co-culture have been deposited at GenBank

under accession numbers MN381734 and MN381735, respectively. The iTAG sequences from 3 different enrichments has been deposited at SRA under accession numbers SRR10031198-SRR10031200. Genome sequences of the co-culture, from which the genome of Ca. M. noduliformans was reconstructed, have been deposited under BioSample SAMN12638105 with raw sequences deposited at SRA under accession number SRR10032644; the reconstructed genome of Ca. M. noduliformans has been deposited at DDBJ/ENA/GenBank under accession number VTOW00000000. Genome sequences of R. lithotrophicus strain RBP-1 have been deposited under BioSample SAMN12638106 with raw sequences deposited at SRA under accession number SRR10031379; the reconstructed genome of R. lithotrophicus strain RBP-1 has been deposited at DDBJ/ENA/GenBank under accession number VTOX00000000. Additionally, reconstructed genomes have been deposited in Joint Genome Institute (JGI) Genomes Online Database Study ID Gs0134339, with Integrated Microbial Genome ID 2784132095 for Ca. M. noduliformans and ID 2778260901 for R. lithotrophicus strain RBP-1. Transcriptome sequence data for the 7 biological replicates have been deposited at SRA under accession numbers SRR10060009, SRR10060010, SRR10060011, SRR10060012, SRR10060013, SRR10060017, SRR10060018. Unique biological materials are available upon reasonable request.

Field-specific reporting

Please select the one below that is the best fit for your research. If you are not sure, read the appropriate sections before making your selection.

☒ Life sciences ☐ Behavioural & social sciences ☐ Ecological, evolutionary & environmental sciences

For a reference copy of the document with all sections, see nature.com/documents/nr-reporting-summary-flat.pdf

Life sciences study design

All studies must disclose on these points even when the disclosure is negative.

Sample size	No statistical methods were used to predetermine sample size. "Sample" as intended here seems to more relevant for the concept of deciding sample size in terms of numbers of animals or human subjects to include in a study. Here, as a microbiologist, we are almost always dealing with populations of tens of millions or more, its really quite a different issue. Aside from that, "sample" means very different things in different contexts, and it is not clear at all how statistics would replace sound experimental design in many of them. We have looked at the Nature document that details a past questionnaire, and see several well articulated responses from colleagues that touch on this.
Data exclusions	No data were excluded in the results. No data exclusion criteria were pre established. Again, it seems this tailored for larger studies on animals and human subjects, and not clear how "pre-establishing" would come into play here.
Replication	Technical and biological replication was performed as indicated in individual experiments reported. All attempts at replication were successful.
Randomization	Randomization was not relevant to this study, it was not a randomized controlled trial. As a standard in microbiology, samples were obtained from a larger population of an enrichment culture to inoculate experimental groups.
Blinding	None. This was not a clinical trial or a randomized controlled trial.

Reporting for specific materials, systems and methods

We require information from authors about some types of materials, experimental systems and methods used in many studies. Here, indicate whether each material, system or method listed is relevant to your study. If you are not sure if a list item applies to your research, read the appropriate section before selecting a response.

Materials & experimental systems

n/a	Involved in the study
☒	☐ Antibodies
☒	☐ Eukaryotic cell lines
☒	☐ Palaeontology
☒	☐ Animals and other organisms
☒	☐ Human research participants
☒	☐ Clinical data

Methods

n/a	Involved in the study
☒	☐ ChIP-seq
☒	☐ Flow cytometry
☒	☐ MRI-based neuroimaging